University of Stavanger

FACULTY OF SCIENCE AND TECHNOLOGY

MASTER'S THESIS

Study program/Specialization: M.Sc. Petroleum Technology/ Reservoir	Spring Semester, 2019 Open access
Author: Marie Tønnessen	Marie Tønnessen (signatures of author)
Supervisors: Aksel Hiorth (University of Stavanger), Kåre Langaas (Aker BP) and Arne Stavland (Norce)	
Title of master`s thesis: **Water shut-off with polymer – core study application for the Alvheim Field**	
Credits(ECTS): 30	
Key words: Disproportionate permeability reduction, polymer, water shut-off, residual resistance factor, filter cake, thermal stability	Total Pages: 71 Stavanger, 15/06/2019

Master's thesis

Water shut-off with polymer - core study application for the Alvheim Field

Marie Tønnessen

June 15, 2019

Abstract

This thesis is an experimental study where different polymers have been evaluated for disproportionate permeability reduction (DPR) effects. The laboratory work was performed at Norce, for Aker BP, as a part of the Master's degree program in Petroleum Technology at the University of Stavanger (UiS).

The main goal was to give additional support to an earlier experimental research initiated by Aker BP. In 2014 during a well intervention, Flowzan was injected into a Kneler well on the Alvheim field. Normally starch-based polymer was used for this type of well intervention, but this time, Flowzan was injected by a mistake. Results from this operation showed reduced productivity of the well and a reduced fraction of water. These results triggered a more in-depth study to investigate if Flowzan could be used as a method for water shut-off. Since Aker BP is planning a new pilot to inject polymer on the Alvheim field, the experimental work in this thesis was to test different polymers for DPR effects.

The laboratory work included viscosity measurements, filtration tests and core flood experiments. The experiments were performed on four polymers; three different versions of Xanthan (Flowzan, Barazan and FDP-S1235-16) and one type Scleroglucan (CS6). The polymers were diluted in Alvheim Formation Water (AFW). Simple filtration tests were performed for each polymer at three different pressures (10, 20 and 50 bar) with respectively three different filter sizes (41, 20, 8 μm), at 20 °C. The same filtration test with 50 bar and filter size 8 μm, was performed at 70 °C with Flowzan and CS6. Core flood experiments with Flowzan, Barazan and CS6, were the last part of the laboratory work. Polymer injection, and backflooding with AFW and Isopar, were performed at Alvheim reservoir temperature, 70 °C. Two core flood experiments were completed for Flowzan injection, one experiment for Barazan injection, and one experiment for CS6 injection. After polymer injection and backfloooding with both AFW and oil, the cores were divided in four segments, and each part were separately backflooded with AFW.

Viscosity measurements showed that the viscosity for all Xanthan polymers were the same, while Scleroglucan had a lower viscosity. From the filtration tests at 20 °C, Flowzan and Barazan indicated some plugging of the filter while CS6 showed total plugging. Filtration

tests (with 50 bar and filter size 8 μm) at 70 °C showed that Flowzan still plugged in the filter while CS6 had excellent filtration. Results from core flooding experiments showed that Flowzan and CS6 plugged into the core, but positive DPR effect ($RRF_o < RRF_w$) was only shown for Flowzan. Barazan showed low plugging in the core, and $RRF_o > RRF_w$. Visual inspections of the treated cores with Flowzan and Barazan revealed filter-cake formation at the core inlet. From the four segments, it was observed that the water permeability increased with the distance moving from the inlet, i.e. the permeability reduction depends on invasion depth.

Since all Xanthan polymers had the same molecular weight but different plugging properties, plugging can be explained by impurities/debris attached to the polymer. These impurities depends on the treatment processes of the polymer product and may vary from different vendors. Since poor filtration was caused by impurities, it is very important to perform a filtration test before a polymer product is selected for a DPR treatment.

The life-time of Xanthan and Scleroglucan was also of interest. An estimation of the life-time assumed that long-term thermal stability tests could be matched with an exponential decay. From this decay it was observed that even though Scleroglucan have been reported a higher thermal stability, Xhantan at 70 °C should last for several years.

Thus, from this laboratory work, Flowzan was recommended as the best candidate for disproportionate permeability reduction treatment at the Alvheim Field (at 70°C). Zones and baffles in the Alvheim reservoir makes it possible to reduce the fraction of water and can contribute to increased oil reserves where zones with remaining oil and low pressure support can be produced more efficient.

Acknowledgements

This laboratory work has been a great learning experience for me. I am very grateful for Aker BP providing me with this exciting work. At Norce, I have felt both welcomed and safe, and friendly treated by everyone. I am very thankful for everyone who has contributed and dedicated their time and work to this master's thesis.

Particular gratitude are expressed to my supervisors; Aksel Hiorth from the University of Stavanger, Kåre Langaas from Aker BP and Arne Stavland from Norce. All of my supervisors have shown great involvement in this work. I appreciate the guidance for a theoretical understanding of the work by Aksel Hiorth and Arne Stavland. They have been supportive and available at all times for comments and questions. In addition, I want to thank Kåre Langaas for all the theoretical guidance and support from Aker BP. It has been a privilege learning from all of them.

At Norce, several people made the laboratory work possible. A great appreciation goes to Daniel Strand, who patiently dedicated his time to explain the equipment and assist during experimental work, Siv Marie Åsen, for providing equipment and theoretical support, and Irene Ringen for guidance of the theoretical work.

Last but not least, I want to thank all the colleagues at Aker BP and Norce for being friendly and supportive during this work.

Contents

List of Tables

List of Figures

Abbreviations

AFW	Alvheim Formation Water
BHP	Bottom Hole Pressure
CDC	Capillary Desaturation Curve
DPR	Disproportionate Permeability Reduction
EOR	Enhanched Oil Recovery
FPSO	Floating Production, Storage and Offloading
FR	Filter Ratio
RF	Resistance Factor
RF_w	Resistance Factor of water
RRF	Residual Resistance Factor
RRF_o	Residual Resistance Factor of oil
RRF_w	Residual Resistance Factor of water
PI	Productivity Index
PI_r	Relative Productivity Index

Chapter 1

Introduction

1.1 Background

During a well intervention in 2014, a commercial Xanthan gum biopolymer was injected in one of the production wells on the Alvheim field. The purpose of the well intervention was to change the production tubing in a well in the Kneler oil accumulation. A polymer was injected to remove all possible hydrocarbons in the tubing before it was pulled out. In this operation a starch-based polymer is normally used to prohibit a negative impact on the production. By a mistake, Xanthan biopolymer Flowzan was injected instead of the starch-based polymer. Two viscous pills with each a polymer concentration of 10000 ppm were bull headed down the well.

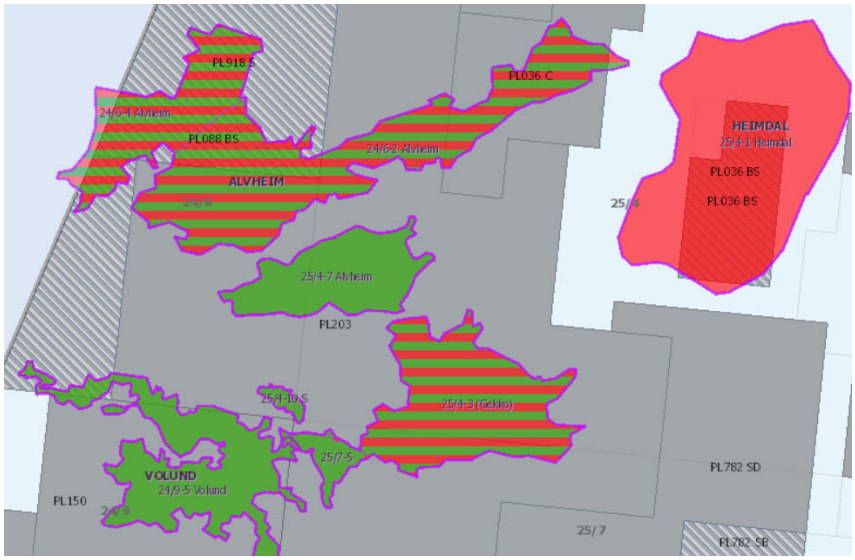

Figure 1.1: Alvheim field [Oljedirektoratet, 2019]

After this operation it was observed that the productivity of the well was reduced with around 50 %. The Kneler well had a relative low productivity index before this operation, hence, this observation was seen as very negative.

Alvheim is an offshore field in the North Sea located on the Norwegian blocks 24/6 and 25/4. With an ownership of 65 % is Aker BP the operator of the field, ConocoPhillips and Lundin holds respectively 20 % and 15 % of the ownership. Versus Petroleum is owner of the UK portion of Alvheim, a part of Boa accumulation that extends into the UK sector. The field arise from Paleocene age and are producing hydrocarbons from sandstones in Heimdal formation. Reservoirs are located at depths of 2100-2200 meters and are formed from submarine fan deposits. The deep marine fans are deposited over the downfaulted axial part of the Jurassic Central Viking Graben. The quality of the reservoir is good and net to gross values are between 80-90 %, porosity is up to 35 % and permeabilities are up to 3 Darcy [Langaas and Stavland, 2019]. Excellent support from an underlying aquifer contributes to a natural flow of hydrocarbons [Norsk Petroleum, 2019]. (An aquifer can be described as a water zone below the reservoir that provides natural pressure support.) Alvheim FPSO are producing hydrocarbons from the Alvheim field (Boa, Kneler and Kameleon), Bøyla, Vilje and Volund fields that are tied up to the FPSO. Production of the field started in June 2008. After 10 years production on Alvheim, water production starts to affect the production of oil.

In 2014, some time after the Flowzan injection, it was noticed that the fraction of water for the Kneler well was reduced. The reduction in water-cut presented potentially 3 MMSTB of extra oil recovery, which was great news [Langaas and Stavland, 2019]. Production from the treated well continued for a period of three and a half year before new changes in the well showed that both the productivity of the well and the fraction of water was higher. From these observations (higher water-cut and higher productivity) it was concluded that the biopolymer was decomposed because of biological degradation (bacterial attack).

High water-cut and unwanted water production is one of the biggest problems in mature oil and gas fields in the petroleum industry [Simjoo et al., 2007]. Fluids will naturally follow the path with the least resistance, where these channels often are created by the heterogeneous nature of a porous rock [Thomas et al., 1998]. Water is more mobile than oil, and in many situations water will dominate the flow through these channels. The produced water is of no direct use, often it contains contaminants and it needs to be re-injected due to environmental concerns. It is therefore of great economic and environmental interest to reduce the amount of water produced. Since it is not possible to know how the Kneler well would have produced today without any injection of polymer, it is difficult to announce an exact value of the Flowzan injection. A forecast is shown in Figures 1.3 and 1.2. The red dotted line represents production without polymer injection,

which is compared to an extrapolated black line of water-cut and oil production after the polymer was injected. The difference between the red-dotted line and the black line, indicates a lower water-cut and a higher oil production after Flowzan polymer injection [Langaas and Stavland, 2019].

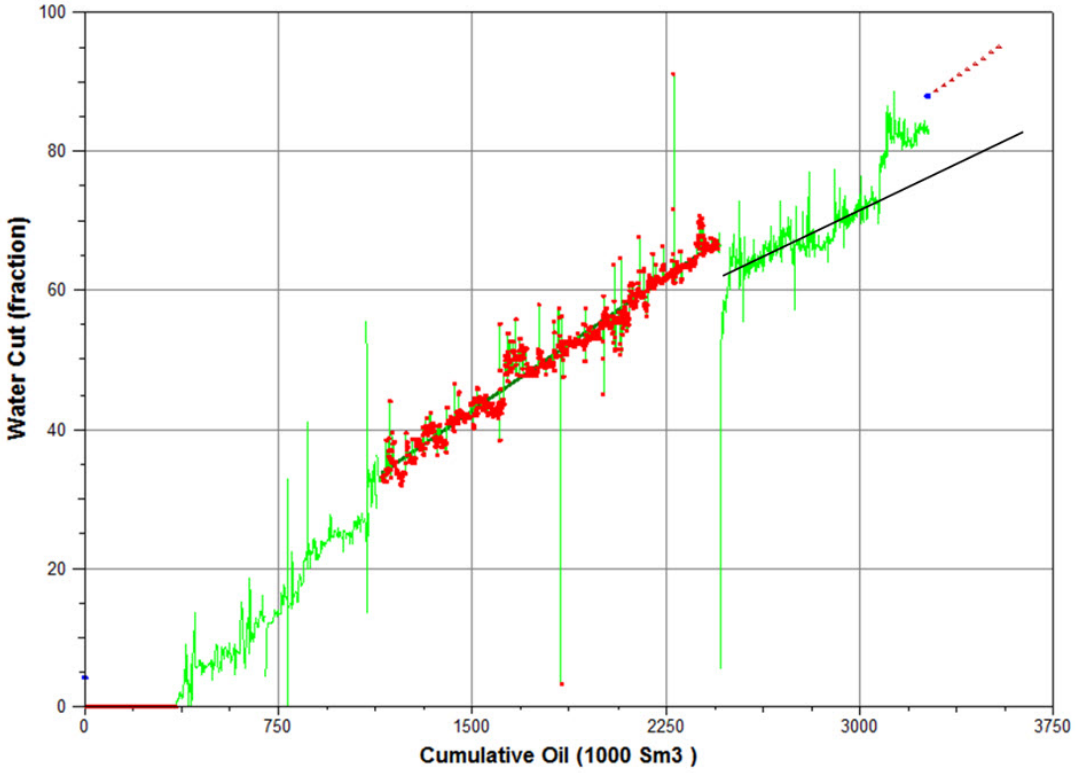

Figure 1.2: Kneler well, water-cut vs. cumulative oil. Red-dotted line is a forecast of water-cut without polymer injection while black line is water-cut with polymer injection, [Langaas and Stavland, 2019].

There are different methods available for water shut-off treatments, both mechanical and chemical methods. The mechanical methods which involve drilling horizontal wells, multilateral wells or use of down hole separation equipment are often expensive. Several chemical methods have been used where gel polymer treatment is one of the most useful methods to reduce water production. The polymer gel have the properties to block certain fractures in the porous rock, and hence, change the fluid flow from areas of low drag to areas of lower permeability with higher drag [Thomas et al., 1998]. Chemical treatment with polymer solutions can also be used in as an improved oil recovery method in both production and injection wells [Simjoo et al., 2007]. The subsea wells installed on Alvheim have long horizontal branches and are completed with sand screens. In these wells, mechanical water shut-off methods are close to impossible and also very expensive, therefore, other methods are of big interest. Water shut-off with polymer on the Alvheim field can be valuable and make a great impact on the production. Zones and baffles in the reservoir

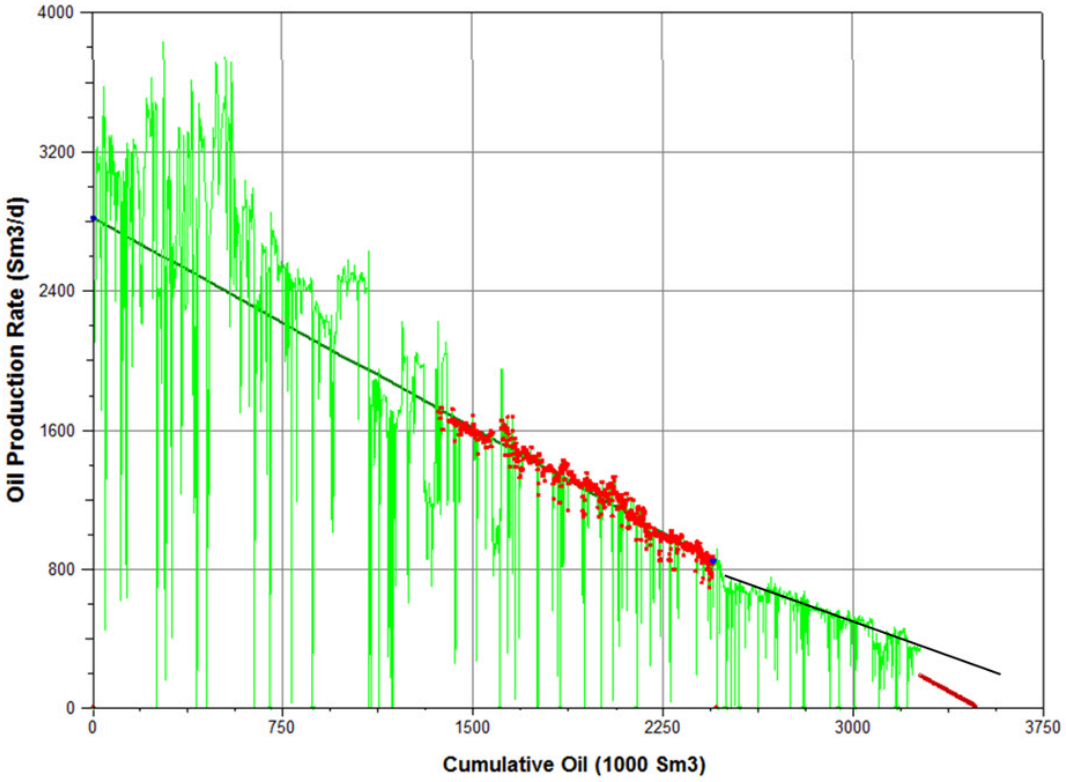

Figure 1.3: Kneler well, oil rate vs. cumulative oil. Red-dotted line is a forecast of oil production without polymer injection while black line is oil production with polymer injection, [Langaas and Stavland, 2019].

makes it possible to reduce the fraction of water and may help us achieve increased oil reserves where the zones with remaining oil and low pressure support can be produced more efficient.

1.1.1 Earlier laboratory work

The observations of reduced water-cut and increased oil recovery potenital in the Kneler well initiated an experimental research project at IRIS in 2017. It was fundamental to understand the changes in the field and see if the biopolymer Flowzan could have a potential for conformance control to reduce water production.

The project was based on filter tests and core flood analysis. Results from this laboratory work showed that the polymer Xanthan (Flowzan) was acting as a filter where the water was obstructed but the oil still managed to finger through. This was good results considering disproportionate permeability reduction (DPR); where many water-soluble polymers have the effect to reduce the permeability of water flow to a greater extent than i.e oil. The permeability reduction for water was a stable factor of 100-450, while the factor for

oil was in between 2-10 and decreasing with time [Langaas and Stavland, 2019].

1.2 Structure and motivation for this thesis

The purpose of this thesis was to investigate in more detail the permeability reduction effects of polymers, and their stability. This should give additional support to the earlier laboratory work, by Aker BP.

Four different polymer products were tested for disproportionate permeability reduction effects. Since the commercial Xanthan gum biopolymer, Flowzan, was decomposed after 3.5 years, the life time of these polymers were also of interest. Aker BP is now planning a new pilot on the Alvheim field where the intention is to inject polymer in the same production well as before. The goal is to increase the oil production and reduce the production of water by create a similar effect as before; water permeability reduction with polymer. The question is, which polymer type will be the best to use for this type of treatment?

For evaluation of DPR effects, different parameters were measured and compared for the different polymers. Filtration tests were important for the evaluation of plugging properties at different filter sizes. These tests also show the temperature dependent polymer behaviour, where it is known that the viscosity of polymer is a function of temperature. Viscosity measurements were carried out for all polymer solutions to easily illustrate the difference in viscosity and molecular weight.

To best match the reservoir conditions, core flood experiments were performed at 70°C, which is the reservoir temperature at the Alvheim field. Before polymer injection, permeability and saturation of oil and water were measured, and also porosity and pore size distribution. This provided information about the cores that were used. During both polymer injection and backflooding (with AFW and Isopar-H), flow rate and pressure were monitored. From this part of the experiment, resistance factor (RF) and residual resistance factor (RRF) were obtained. RRF values were important for the DPR evaluation and indicated if the treatment had been successful. For a successful treatment, water production should be reduced and the productivity of oil should increase.

This thesis consists of a theoretical part relevant for the laboratory work. The laboratory work is described where an experimental procedure have been listed. The experimental results will be presented, and in the final part we discuss the measured parameters in a larger scale.

Chapter 2

Theoretical background

2.1 Flow in porous media

Flow in a porous media have been studied by Henry Darcy, and an expression can be defined by Darcy Law. The law describes a linear, horizontal flow for an incompressible fluid. In a generalized form, this equation can be written as follows [Zolotukhin and Ursin, 2000]:

$$q = -\frac{kA}{\mu}\frac{dp}{dx}, \tag{2.1}$$

where q is the flow through a homogeneous and horizontal porous media for a single phase. The flow depends on absolute permeability, k, and cross-section area, A. μ, is the viscosity of the fluid and, ΔP, is pressure drop between inlet and outlet of the medium. Pressure decreases in direction of flow which means that the pressure gradient becomes negative in the flow direction [Zolotukhin and Ursin, 2000].

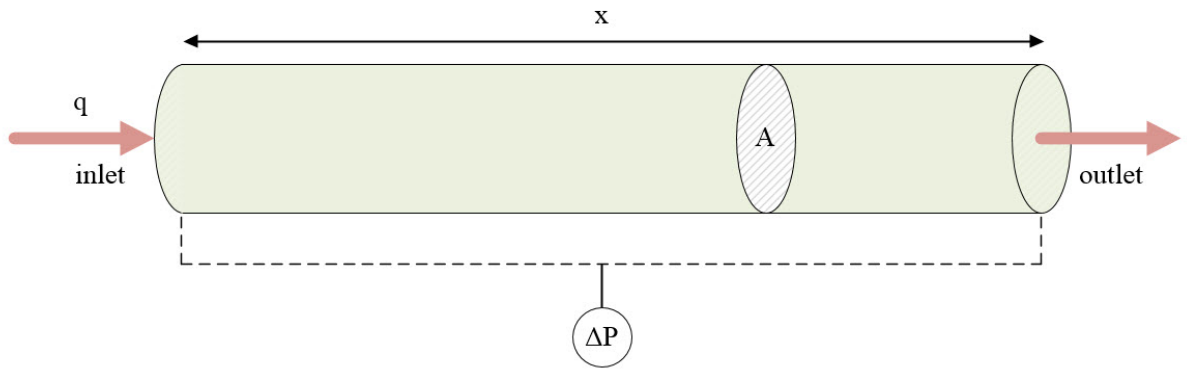

Figure 2.1: Flow through a homogeneous porous media for a linear and horizontal flow.

2.1.1 Harmonic average

In this thesis, during the core flooding experiments, the cores will be divided in several parts. In section 3.5, it is described that permeability and residual resistance factor (see section 2.4.1) were calculated from layers connected in series. An average value of layers connected in series is called a harmonic average and will be explained below.

For a flow through different zones that are connected in series, as shown in Figure 2.2, the harmonic average gives the effective parameters. For a zone, i, flow rate through this zone is given:

$$Q = \frac{k_i A}{\mu} \frac{\Delta P_i}{L_i}, \tag{2.2}$$

where, ΔP_i, is the pressure drop over layer i and, L_i, is the length.

The total pressure drop over the whole series follows as the sum of individual pressure drops:

$$\Delta P_{tot} = \sum \Delta P_i = \frac{Q\mu}{A} \sum \frac{L_i}{k_i}, \tag{2.3}$$

and hence, by Darcy Law (Equation (2.1)) on the total system, it follows that the average permeability is:

$$k_{avg} = \frac{L_{tot}}{\sum \frac{L_i}{k_i}}, \tag{2.4}$$

This average is called the harmonic average, for linear geometry
[Kantzas, A and Bryan, J and Taheri, S,].

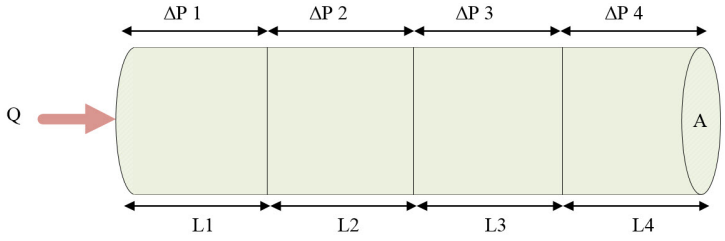

Figure 2.2: Layers connected in series

From Equation (2.25), an expression for residual resistance factor is given. By using this definition, a harmonic average of RRF can be defined for the total series:

$$RRF_{avg} = \frac{\sum(L_i RRF_i)}{\sum L_i}. \tag{2.5}$$

2.1.2 Viscous flow in a capillary tube

Darcy law is not valid for non-Newtonian fluids, and to gain more insight we will look at a capillary tube model. Laminar flow for a Newtonian fluid is presented before the non-Newtonian polymer situation in section 2.1.3.

When a fluid is flowing there will appear frictional interaction between the fluid molecules, which acts as a force resisting the flow. Viscosity is the measure of this internal resistance of a fluid when shear is applied. For Newtonian fluids, viscosity can be expressed by linking the shear stress tensor, τ, with the resulting shear rate, $\dot{\gamma}$. Shear rate is defined as $\dot{\gamma} = \frac{dv}{dr}$ and the applied shear stress, τ, is given by:

$$\tau = \mu\dot{\gamma}, \tag{2.6}$$

where, μ, is fluid viscosity and, γ, is shear rate depending on fluid flow velocity. Viscosity, μ, is then given with the same parameters used in Equation (2.6) [Zolotukhin and Ursin, 2000]:

$$\mu = \frac{\tau}{\dot{\gamma}}. \tag{2.7}$$

For a viscous flow in a cylindrical tube of radius R, a laminar flow can be defined by introducing Hagen-Poiseuille's equation [Zolotukhin and Ursin, 2000]:

$$q = \frac{\pi R^4}{8\mu}\frac{\Delta P}{\Delta L_t}, \tag{2.8}$$

where $A = \pi R^2$ is the cross-sectional area of the capillary tube, and μ, is viscosity.

The average velocity in the tube can be derived [Zolotukhin and Ursin, 2000]:

$$v_{avg} = \frac{q}{\pi R^2} = \frac{R^2}{8\mu}\frac{\Delta P}{L_t}, \tag{2.9}$$

Equation (2.9), describes the average flow velocity for a Newtonian fluid in a tube for a laminar flow pattern.

To describe the flow behavior in a porous media, the simplest way is to use a capillary bundle model. Assume the porous media is a bundle of parallel capillary tubes, all with

the same radius, illustrated in Figure 2.3. Then a total flow rate through the media can be written as:

$$Q = \sum q = Nq = \frac{N\pi R^4}{8\mu}\frac{\Delta P}{L_c}, \tag{2.10}$$

where, N, is the number of capillary tubes, R, is the radius and L_c is the length of the tube.

From definition of porosity, ϕ, it is known that:

$$\phi = \frac{V_p}{V_b} = \frac{N\pi R^2 L_c}{AL}, \tag{2.11}$$

where, V_p, is pore volume, and V_b, is the total bulk volume, and hence, an expression for the total number of tubes can be given:

$$N = \frac{\phi AL}{\pi R^2 L_c}. \tag{2.12}$$

A new expression for flow is expressed:

$$q = \frac{\phi R^2 AL}{8\mu}\frac{\Delta P}{L_c^2}, \tag{2.13}$$

then by multiplying Equation (2.13) with $\frac{L}{L}$, flow rate is expressed with the tortuosity parameter, τ:

$$q = \frac{\phi R^2 A}{8\mu\tau^2}\frac{\Delta P}{L} = \frac{kA}{\mu}\frac{\Delta P}{L}, \tag{2.14}$$

where $\tau = \frac{L_c}{L}$, and k, is given as:

$$k = \phi\frac{R^2}{8\tau^2}, \tag{2.15}$$

where permeability, k, is expressed with porosity and the pore size (R) [Lake, 1989].

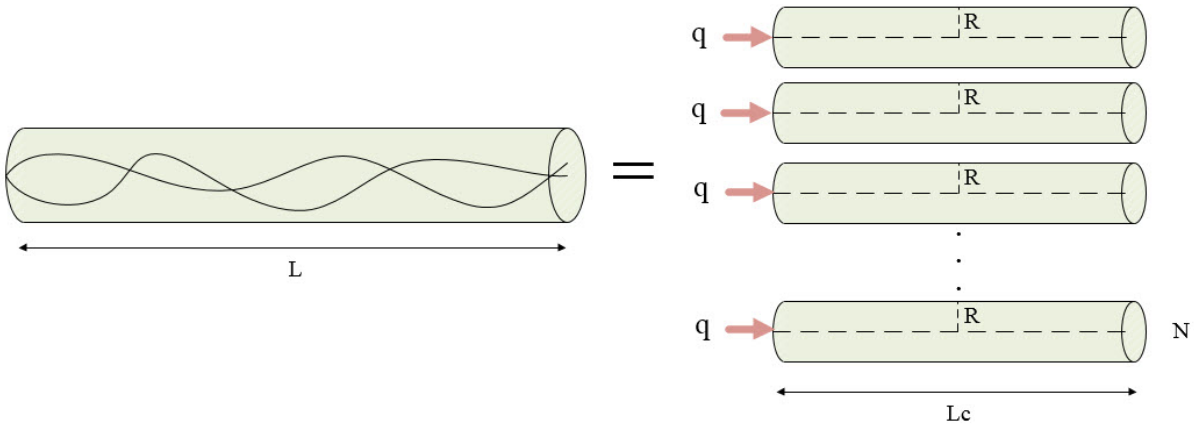

Figure 2.3: Illustration of a capillary bundle model, where Lc>L.

2.1.3 Non-Newtonian flow

In a porous media, the flow is not well-defined and a polymer flow through a porous core will differ from the flow measured in rheometers. Microscopic structure and geometry of the porous media are important factors, and the flow through this media will be a lot more complex. A relationship between the polymer flow behaviour in a porous media and the bulk rheological behaviour have been studied [Askarinezhad, 2018].

Some fluids are non-Newtonian fluids, hence, the viscosity term, μ, from Equation (2.6) is not constant. [Sun et al., 2012]. Polymers in general are non-Newtonian fluids and for these type of fluids the viscosity does not remain constant at different shear rates. In other words the viscosity will change when different forces are applied to the fluid and it is said to be shear-dependent. The viscosity will decrease as the shear rate is increased. This is called a shear-thinning behaviour, shown in Figure 2.4.

For a non-Newtonian fluid, shear stress can be defined as follow:

$$\tau = K\dot{\gamma}^n, \tag{2.16}$$

where, K, and n, are constants.

Since non-Newtonian fluids are shear-thinning, the apparent viscosity is decreasing when shear rates are increasing:

$$\mu = \frac{\tau}{\dot{\gamma}} = K\dot{\gamma}^{n-1}. \tag{2.17}$$

Equation (2.17) is known as the Power-law model. In this model, μ, is the apparent

viscosity, $\dot{\gamma}$, is the shear rate, and both, K, and n, are constant parameters where $n < 1$. For shear rates where viscosity have shifted from Newtonian to shear-thinning viscosity, the viscosity matches this Power-Law equation above [Askarinezhad, 2018]. For shear rates where viscosity have shifted from Newtonian to shear-thinning viscosity, the viscosity matches this Power-Law equation above [Askarinezhad, 2018]. For a Newtonian fluid where K is the constant viscosity and n is equal to 1 the expression will form Newtons Law:

$$\tau = k\dot{\gamma}, \tag{2.18}$$

where the linear relationship between shear stress, τ, and shear rate, $\dot{\gamma}$, that exists for the Newtonian fluids are defined. The constant viscosity of a Newtonian fluid when a force is applied is also shown in Figure 2.4.

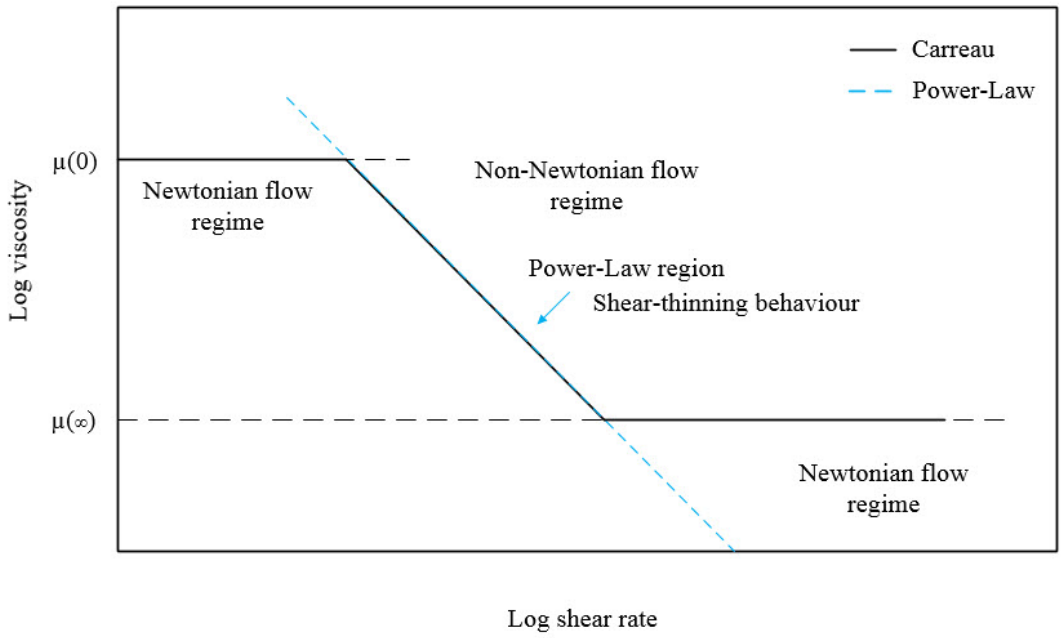

Figure 2.4: Viscosity vs. shear rate with logarithmic scales. Illustrating polymer behaviour when shear rates are applied to a polymer.

Another model represented in the literature is the Carreau model. Since polymers behave like Newtonian fluids when very low or very high shear rates are applied, the Power-Law model can only be applied at intermediate shear rates where a shear-thinning behavior appears. To describe the behavior of polymer solutions for all shear rates Carreau model have been presented [Byron Bird et al., 2018]:

$$\frac{\mu - \mu_\infty}{\mu_0 - \mu_\infty} = [1 + (\lambda\dot{\gamma})^2]^{(n-1)/2}, \tag{2.19}$$

where following parameters are included:

- viscosity, μ
- Viscosity at zero shear rates, μ_0
- Viscosity at infinite shear rates, μ_∞
- relaxation constant, λ
- shear rate, $\dot{\gamma}$
- power-law exponent, n, where $n < 1$

In a porous medium, shear rate and viscosity will not be constant. Effective shear rate is proportional to flow rate and different models have been suggested where $\dot{\gamma}$ is a function of flow rate and properties of the porous media. Based on the capillary bundle model mentioned earlier, the wall shear rate, $\dot{\gamma}$, in a capillary tube can be defined as follows:

$$\dot{\gamma}_{wall} = \frac{4v_{avg}}{R} = \frac{4q}{AR}. \tag{2.20}$$

Definition for pore size radius, Equation (2.15), can be inserted into Equation (2.20) and shear rate can be expressed by:

$$\dot{\gamma} = \frac{4v}{\tau}(\frac{\phi}{8k})^{1/2} = \frac{4q\alpha}{A\sqrt{8k\phi}}. \tag{2.21}$$

This definition of shear rate is useful when rheological properties of non-Newtonian fluids in permeable media flow are predicted and correlated. Where, $v = q/A\phi$, is the pore velocity. α is a constant related to the type of porous media and the pore geometry. For a bundle of capillary tubes, α=1. For unconsolidated sand, 1.05> α <2.5, and 1.4> α <14.0, for consolidated sand.

2.2 Polymers

Polymers are compounds that consists of chain molecules. They are created via polymerization of many small structural units, called monomers. The molecular weight of a polymer molecule is given by the molecular weight of the structural unit and the number of these units in the polymer molecule [Byron Bird et al., 2018]. Because of the polymers large molecular mass compared to their small molecule compounds they have unique

properties and a special rheology. Rheology describes the flow behaviour and estimate the deformation when a force is applied [Anton Paar Wiki, 2019]. At low shear rates, polymers behave like Newtonian fluids because molecules are rotating at a constant velocity, hence, there is no significant change in the structure and the viscosity remains constant. When shear rate is increased, molecules will orient themselves in the flow direction and/or they will start to deform. This leads to a reduced interaction between the molecules which will cause a slow reduction of viscosity; a shear-thinning behavior. For high shear rates, polymer starts to act as a Newtonian fluid again. In this flow, all the molecules are oriented in the flow direction and are not affecting the viscosity. Note that viscosity are lower for this flow regime [Zolotukhin and Ursin, 2000].

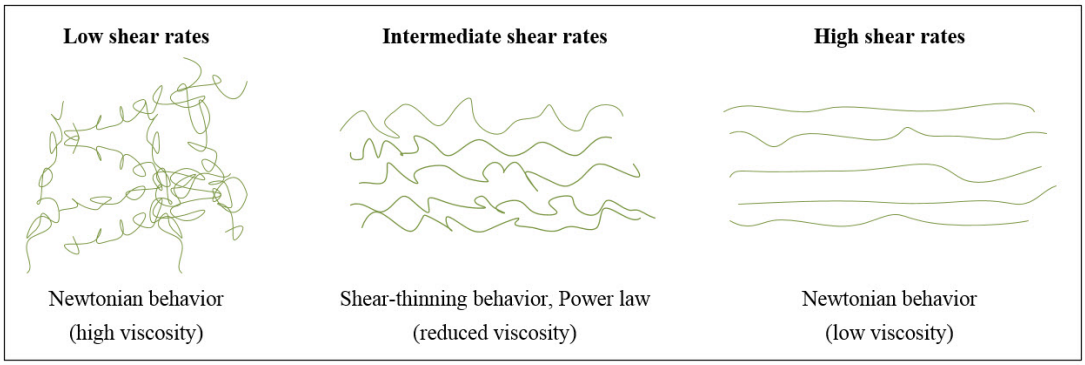

Figure 2.5: Molecule orientation of polymers and flow behaviour under different shear rates.

There are both synthetic polymers and naturally occurring polymers, also called biopolymers. Generally, biopolymers contains a large number of different structural units, compared to synthetic biopolymers. Biopolymers are environment friendly and have been used as additives in well fluids and drilling operations. Viscoelastic properties are important when polymers are evaluated as methods for increased oil recovery during different production stages in the petroleum industry. The main reason for use of polymers is to increase the viscosity [Askarinezhad, 2018]. Polymers have been used in offshore reservoirs to improve the sweep efficiency and to achieve favorable flow properties. When viscosity of the injected water is increased by polymer, the tendency of water to finger through the oil will be reduced and hence the injected water will sweep more oil towards the production wells and improve recovery [Abidin et al., 2012]. Operations like this is called enhanced oil recovery (EOR) polymer flooding, where EOR is appearing from injected materials that are not normally existing in an oil reservoir [Sydansk and Romero-Zerón, 2011]. Polymers can be used in different operations, and hence, their properties differs. While an EOR polymer should increase viscosity and create a more uniform flow in a porous rock, a polymer used for example to control fluid loss should build up a filter cake at the surface of the rock to prevent further invasion of filtrate and avoid lost fluid. Polymer properties

can also be suitable for disproportionate permeability reduction treatments, this is further described in section 2.3.

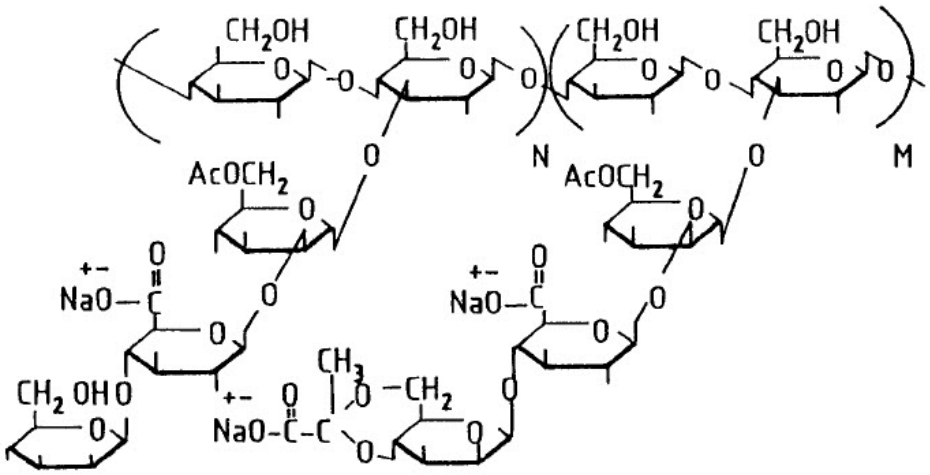

Figure 2.6: Xanthan molecule structure, [Littmann et al., 1992].

Xanthan biopolymer is a polysaccharide produced by xanthomonas campestries bacteria. Molecules are stabilized by hydrogen bonds and the structure is rigid. Scleroglucan is a polysaccaride glucan produced by fungus Sclerotium rolfsii bacteria. Molecule structure of this polymer will form a rigid triple helix. Scleroglucan is more thermal stable than Xanthan, this is further described in section 2.5.

Molecule structure of Xanthan and Scleroglucan are shown in Figures 2.6 - 2.7. Both, Xanthan and Scleroglucan, are environmentally friendly. To prevent biodegradation in oil reservoirs, biocide can be added to the solution.

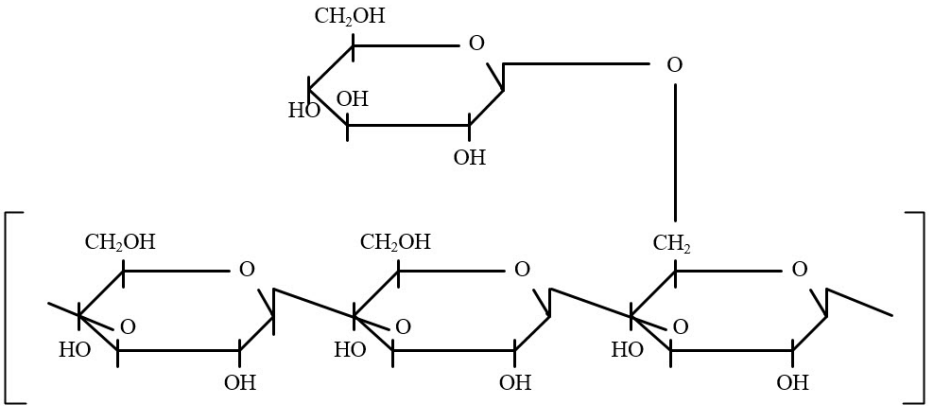

Figure 2.7: Scleroglucan molecule structure.

2.3 Conformance control

"The term conformance in its truest and original form is defined as the measure of the volumetric sweep efficiency during an oil-recovery flood or process being conducted in an oil reservoir" [Sydansk and Romero-Zerón, 2011]. The volumetric sweep efficiency introduce the amount of pore volume that is swept by the injected fluid in percent (%), or as a fraction. It can be written as E_V and is expressed by:

$$E_V = E_A E_I. \tag{2.22}$$

In this formula E_A is the areal sweep efficiency, and E_I is the vertical sweep efficiency [Sydansk and Romero-Zerón, 2011].

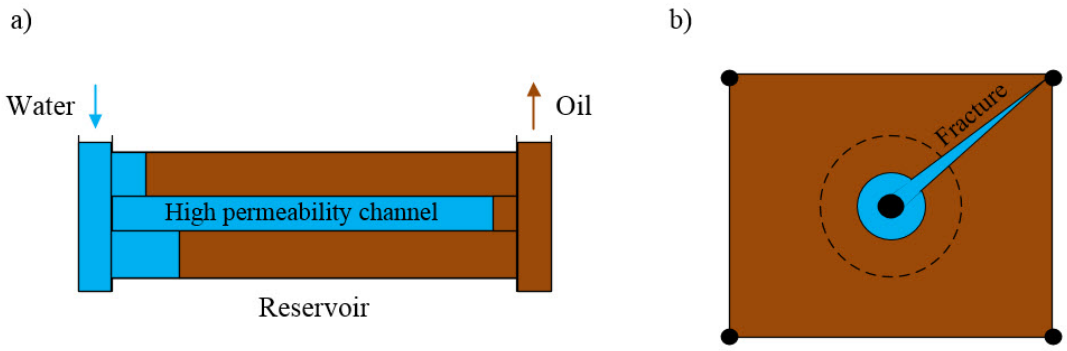

Figure 2.8: Conformance problems: a) vertical conformance problem with one producer and one injector, b) areal conformance problem with four producer wells and one injector.

Figure 2.8 illustrates two conformance problems where we have poor vertical sweep and poor areal sweep. This problem can occur in reservoirs with high-permeability channels or with fractures in the formation. Water will typically flow through the high permeable zones, especially when water is more mobile than oil. Hence, a large amount of oil will be left in the reservoir. For a porous medium, viscous fingering will increase as the viscosity of the displacing fluid is decreased, and hence the sweep efficiency will be poor. By adding polymer to the injected water the viscosity of the displacing fluid will be increased, and mobility reduced. In a reservoir with a given degree of permeability heterogeneity this will promote a more uniform displacement process and thereby improve the volumetric sweep efficiency, E_V.

Mobility ratio, M, is the term that indicates the stability of a displacement process and defined as:

$$M = \frac{\lambda_D}{\lambda_d}, \tag{2.23}$$

where, λ_D, is the displacing fluid's mobility, normally water, and λ_d, is the displaced fluid's mobility which is normally oil. The mobility of a phase i is given:

$$\lambda_i = \frac{k_i}{\mu_i}, \tag{2.24}$$

and the mobility describes the relation between relative permeability, k, and viscosity, μ. For a stable and uniform displacement process, M, is less than 1 and we have a favorable mobility ratio [Sydansk and Romero-Zerón, 2011].

2.4 Water shut-off method

The term conformance control can also refer to a measure of excessive water production and the treatment of this water from petroleum reservoirs. As mentioned earlier, unwanted water production is a problem in the petroleum industry and the problem occurs when the excessive water competes directly with oil production. In reservoirs like this, a reduced production of water can often contribute to a greater drawdown pressure, and hence, increase oil production rates [Sydansk and Romero-Zerón, 2011].

Many polymer gel technologies have been introduced and discussed in the literature for use in water shut-off treatments and for conformance control. Also gas shut-off treatments have been reported [Sydansk et al., 2000]. A treatment where the effective permeability for water is being reduced in a greater extent than the effective permeability for oil is called disproportionate permeability reduction (DPR) treatment [Askarinezhad, 2018]. Many polymers and polymer gels have this property. This type of treatment is done by bullheading polymer solution into the well. This injection method is cheaper than other treatments and there are less operational complexities. Even though the treatment method is beneficial, there are important conditions with DPR treatments; the treatment will be of no value in a reservoir that effectively consist of only one zone. For any success of disproportionate permeability reduction, the hydrocarbon zones must be somewhat isolated from the producing water zones. If oil and water are flowing through the same zone, a permeability reduction will reduce the production of both oil and water. Another case of scenario is reduced productivity of the well at the same water-cut as before. The goal is to achieve a reduced water production without making any damage, or inhibition, on the oil production [Askarinezhad, 2018]. Deep and high productive wells that are

producing light oil and not having too high water-cut are the most suitable well candidates for DPR treatments [Stavland, 2010].

2.4.1 Important parameters

Residual Resistance Factor

There is a quantitative measurement for the effective determination of permeability reduction, called residual resistance factor. This is defined for each phase i flowing in a porous medium, RRF_i. In a system with water and oil where RRF_w is larger than RRF_o, there is a positive effect of disproportionate permeability reduction, which means that the relative permeability of water is reduced in a greater extent compared to the relative permeability of oil. If $RRF_w > 10$ and $RRF_o < 2$ the DPR treatment will also be efficient. Opposite, it will be an ineffective and negative DPR treatment if $RRF_w < RRF_o$ [Askarinezhad, 2018]. The value of residual resistance factor, may also be of much greater value in treated linear flow problems compared to radial flow problems [Seright et al., 2003]. The residual resistance factor is given with the following formula, where permeability from Darcy Law is used:

$$RFF = \frac{k_i}{k_f} = \frac{\frac{\Delta P_{after}}{Q_{after}}}{\frac{\Delta P_{before}}{Q_{before}}}, \tag{2.25}$$

where initial phase permeability, k_i, is divided on final phase permeability, k_f, for the flowing fluid. ΔP_{before}, and ΔP_{after}, are the pressure difference over the porous media before and after polymer injection, and Q is the flow rate for the injected fluid.

Resistance Factor

Another parameter that is often measured from DPR treatments is the resistance factor, RF. Resistance factor is defined as the ratio of mobility of water, λ_w, to the mobility of a polymer solution, λ_p. Both parameters under the exactly same conditions. Then RF is expressed as:

$$RF = \frac{\frac{k_w}{\mu_w}}{\frac{k_p}{\mu_p}} = \frac{\frac{\Delta P_p}{Q_p}}{\frac{\Delta P_w}{Q_w}}, \tag{2.26}$$

where, k, and μ, are phase permeability and viscosity for water (w) and polymer (p) respectively. Differential pressures and flow rates are also given for water and polymer. From relative viscosity, μ_p, polymer viscosity is given by:

$$\mu_p(T) = \mu_r \mu_w(T) = \frac{K}{\mu_w} \dot{\gamma}^{n-1} \mu_w(T), \tag{2.27}$$

where, T, is temperature and, $K\dot{\gamma}^{n-1}$, is polymer viscosity matched with Power-Law, Equation (2.17).

Drawdown pressure and Productivity Index

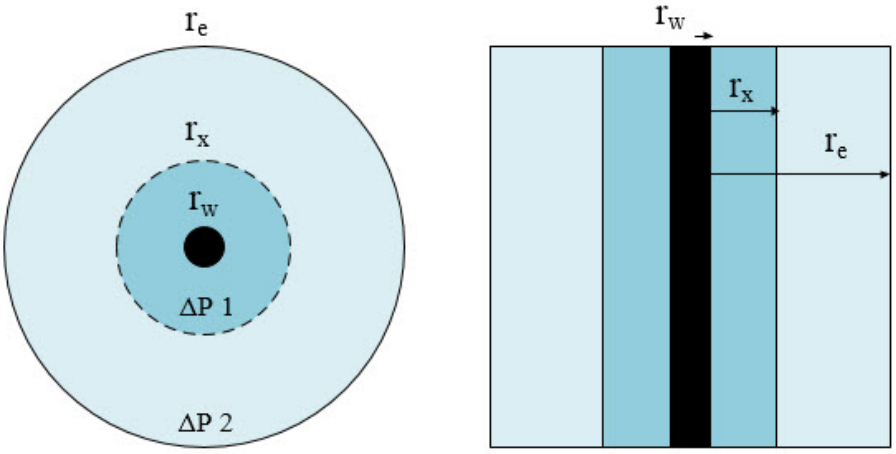

Figure 2.9: Illustration of a radial geometry

Drawdown pressure is also an important parameter. Drawdown pressure is the pressure difference between reservoir and wellbore that contributes to a movement of hydrocarbons into the well. The definition can be expressed by flow rate and productivity index on the form:

$$\Delta P_{drawdown} = \frac{q}{PI}, \tag{2.28}$$

where, q, is the well flow rate and, PI, is the well's productivity index calculated from Equation (2.29).

The productivity of a well define its potential to produce. An estimate can be measured from the following formula:

$$PI = \frac{Q}{BHP_S - BHP_F}. \tag{2.29}$$

The productivity depends on the liquid rate (Q), the bottom hole pressure after a given shut-in period, e.g 24 hours (BHP_S), and on the flowing bottom hole pressure (BHP_F) [Langaas and Stavland, 2019]. This parameter will change with the life-time of the well.

Increased oil production is related to a balance between the oil productivity reduction and the increased drawdown that occurs when water-cut is reduced. An analytical expression in radial geometry for the relative productivity index can be derived (see Figure 2.9 for an illustration of the radial geometry). First, by looking at the pressure difference with and without a damaged zone, ΔP_1 and ΔP_0, we get:

$$\Delta P_1 = \frac{\mu q}{2\pi h \overline{k}} \ln \frac{r_e}{r_w}, \tag{2.30}$$

$$\Delta P_0 = \frac{\mu q}{2\pi h k} \ln \frac{r_e}{r_w}, \tag{2.31}$$

r_w, is the well radius, and r_e, is the external radius in the producing reservoir zone. The permeability $\overline{k}$ is a new permeability describing both the damaged zone and the uninvaded zone (k), and is given by the following equation:

$$\frac{\ln \frac{r_e}{r_w}}{\overline{k}} = \frac{\ln \frac{r_e}{r_x}}{k} + \frac{\frac{r_x}{r_w}}{k_x}, \tag{2.32}$$

where, r_x, is the radius of the damaged zone, and k_x, is the permeability of this zone.

The expression for productivity index is already given in equation (2.29), and if flow rate is the same before and after the treatment, a radial productivity index can be written:

$$PI_r = \frac{PI_1}{PI_0} = \frac{\Delta P_0}{\Delta P_1} = \frac{\overline{k}}{k}, \tag{2.33}$$

where, PI_0, is the productivity before fluid invasion.

By multiplying the equation above with $(\frac{\ln \frac{r_e}{r_w}}{\ln \frac{r_e}{r_w}})$, the expression can be rewritten on the following form:

$$PI_r = \frac{\ln(\frac{r_e}{r_w})}{k(\frac{\ln(\frac{r_x}{r_w})}{k_x} + \frac{\ln(\frac{r_e}{r_x})}{k})} = \frac{\ln(\frac{r_e}{r_w})}{(\frac{k}{k_x} - 1)\ln(\frac{r_x}{r_w}) + \ln(\frac{r_e}{r_w})}. \tag{2.34}$$

$(\frac{k}{k_x}-1)(\ln(\frac{r_x}{r_w}))$ is the same as the skin factor (S). The skin characterizes the well damage and depends on both the permeability reduction and the invasion depth, as shown in the expression. Described in the section above, it is known that $\frac{k}{k_x} = RRF$. Since RRF_w and RRF_o differs, PI_r will be different for water ($PI_{r,water}$) and oil ($PI_{r,oil}$) [Stavland, 2010].

2.5 Thermal stability

Thermal and mechanical stability are important parameters when polymer solutions are evaluated for injection. Reservoir conditions need to be considered since both temperature and salinity will affect the stability of polymers. Compared to synthetic polymers, biopolymers are not sensitive to mechanical degradation. At high reservoir temperature, polysaccharides Xanthan and Scleroglucan are two candidates [Kalpakci et al., 1990]. For Xanthan, temperature stability have been reported between approximately 70 °C and 90 °C, while stability for Scleroglucan are reported in the range from 70 °C to above 105 °C [Zolotukhin and Ursin, 2000].

Thermal stability can be determined by viscosity measurements. Polymer solution is prepared into a cylinder in an anaerobic environment. There are procedures to eliminate polymer aggregates and oxygen. A short-term chemical degradation can be caused by oxygen, while a chemical degradation of the polymer backbone is a long-term attack depending on temperature. A common mechanism for polymer degradation is lowered molecular weight, and hence, reduced viscosity. This can be illustrated in a plot, see Figure 2.10.

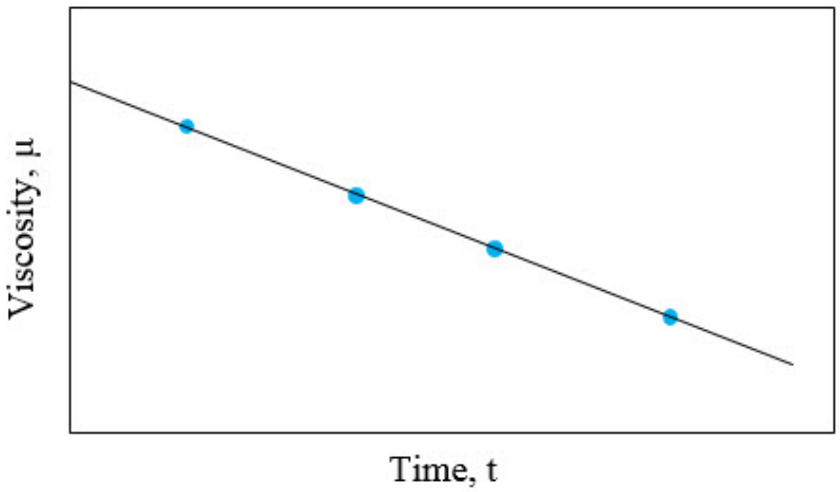

Figure 2.10: Illustration of polymer breakdown; reduced viscosity.

An experimental study of these polymers is reported. In this experiment thermal stability of Xanthan and Scleroglucan without additives were evaluated at different temperatures (93, 100 and 105 °C) [Kalpakci et al., 1990]. Xanthan showed lower thermal stability than Scleroglucan. The viscosity loss of Xanthan varied between 10-90 percent, depending on the source of Xanthan and the test conditions. Scleroglucan, on the other hand, indicated excellent thermal stability. The viscosity loss was small, and even retained at 100 °C over

720 days. The rigid triple helix structure of Scleroglucan may be the reason why this polymer is more thermal stable than xanthan.

Long-term tests of thermal stability can be matched with an exponential decay that gives viscosity, μ:

$$\mu \approx \mu_0 e^{-\lambda t}, \tag{2.35}$$

where, t, is the time, $\lambda = \lambda(T)$ and $1/\lambda$ present the half-life time. Solving for λ:

$$\lambda(T) \approx A e^{\frac{-Ea}{RT}}, \tag{2.36}$$

where, A, is the constant, E_a, is a constant activation energy, R, is the Boltzmann constant and, T, is temperature in Kelvin. Then, the half-life time can be given:

$$\frac{1}{\lambda} \approx \frac{e^{\frac{Ea}{RT}}}{A}, \tag{2.37}$$

From this decay, where half life-time can be plotted against temperature, it is observed that Xanthan at 70°C will last for several years. Since these type of experiments requires years before results are achieved, this is not included in the laboratory work for this thesis.

Biopolymers, or polymers in general, are susceptible to biological degradation, due to bacterial activity. This often occurs in low-temperature reservoir zones. To prevent this bacterial degradation biocides have been effectively used [Zolotukhin and Ursin, 2000].

Chapter 3

Experimental arrangement

3.1 Work flow

The laboratory work has been divided into two parts. The first part consists of viscosity measurements and filter tests, while the second part are core flood experiments based on results from part one. A short description of the laboratory work is given in the following order;

1. Brine that is used to dilute polymer concentrations was mixed. Alvheim synthetic formation water, AFW, is the brine used in all parts of this experiment.
2. Second step was calculation of polymer weight and brine, then polymer solutions were mixed with a polymer concentration of 10000 ppm.
3. Further it was carried out viscosity measurements of all the different polymer solutions, the formation brine and the oils, both marcol and isopar. Simple filter tests were performed on polymer solutions with different filter sizes and at different pressures.
4. The second part of the laboratory work was core flood experiments where several procedures were applied. This experiment was only performed on selected polymer solutions based on filter tests results. This is further described in section 3.5.

3.2 Alvheim formation water and polymer solutions

Alvheim synthetic formation water was created by mixing salts and deionized water. Two 5-liter solutions were made separate and stirred on a magnetic stirrer for at least one hour, see Figure 3.1. The solutions were filtered through a 0.45 μm HAWP filter from Merck Millipore Ltd and mixed together before polymers were dissolved. The composition of salt is shown in Table 3.1.

Table 3.1: Alvheim formation water

Salt	g/l
NaCl	52.317
KCl	0.416
$MgCl_2 \times 6H_2O$	5.018
$CaCl_2 \times 2H_2O$	9.573
$SrCl_2 \times 6H_2O$	1.095
$BaCl_2 \times 2H_2O$	0.374
$Na_2\ SO_4$	0.003
$NaHCO_3$	0.200
TDS	63.482

Four different polymers were used. Three different Xanthan brands (Flowzan, Barazan and FDP-S1235-16) and one type of Scleroglucan (CS6). Flowzan was delivered as dry powder form MI-Swaco, Barazan and FDP-S1235-16 as dry powder from Halliburton and CS6 delivered as dry powder from Cargill. All polymers were dissolved in Alvheim brine with a concentration of 10000 ppm. It was assumed that the polymers have an active polymer concentration of 100% and, hence, the solution of 10000 ppm (or 1wt%) consists of 10.00 g polymer in 990.00 g brine. The polymer and brine were mixed by a Silverson L5M at 5000 rpm for 30 minutes. Silver paper was used on bottle, to avoid evaporation. Polymer and brine distribution are listed in Table 3.2

Table 3.2: Mixed polymer solutions

Polymer type	Weight$_{polymer}$ [g]	WeightAFW [g]
Flowzan	10.00	990.00
Barazan	10.00	990.00
FDP	10.00	990.00
CS6	10.00	990.00

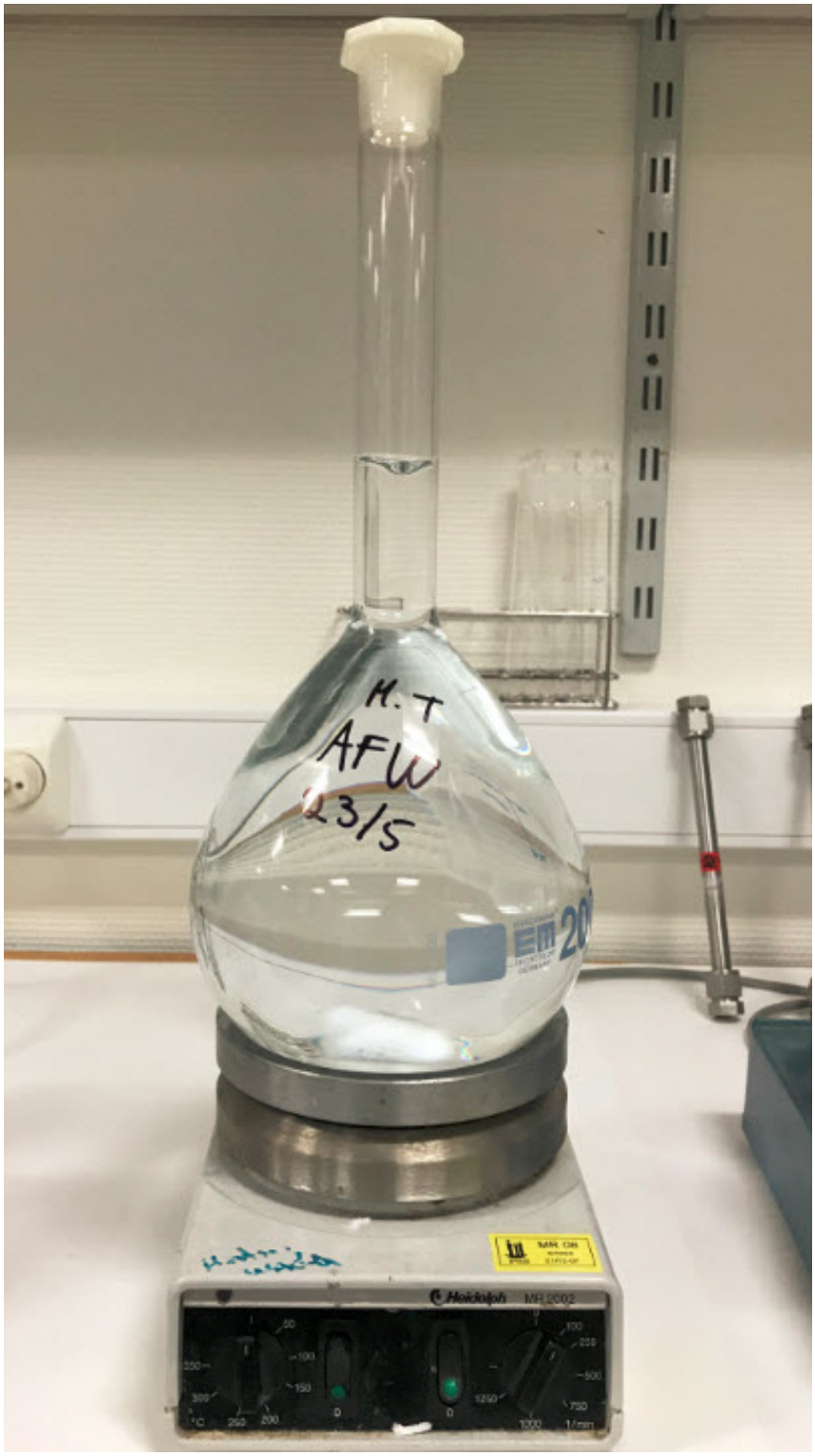

Figure 3.1: Alvheim formation water mixed on a magnet stirrer.

3.3 Viscosity measurements

Anton Paar Physica MCR 301 rheometer with cone-plate geometry was used to measure viscosity, see Figure 3.2. The temperature was set to 20°C with shear rates varying from 0.1 to 500 s^{-1}. New polymer solutions, with the exactly same content as described above, were mixed for each filter tests and for each core flood. Viscosity was measured for all the samples that were used in the experiments.

Figure 3.2: Anton Paar physica MCR 301 rheometer with cone-plate.

3.4 Filter testing

In this experiment, samples with polymer concentration of 10000 ppm was filtered through different filter sizes with different pressures. Both filter sizes and injection pressures was increased compared to the reference polymer filtration test where polymer was injected through a filter size of 5 μm at a constant pressure of 2 bar. The reason for this was a higher polymer concentration in this laboratory work than for standard EOR polymer flooding experiments.

The filter ratio, FR, was calculated from the following formula:

$$FR = \frac{t_3 - t_2}{t_2 - t_1}, \tag{3.1}$$

where t_1, t_2, t_3 was measured time to reach respectively 50, 100 and 150 gram. FR where t_1, t_2, t_3 was measured time to reach respectively 100, 200 and 300 gram was also calculated for polymers that reached this weight. Note that some polymers plugged before 300 (and even 150 gram) gram were reached.

3.5 Core flooding experiment

Three different core flood experiments were performed with Bentheimer sandstone. This sandstone is assumed to be a clean quartz sandstone and contains only traces of other minerals. The cores had a length of 25 cm and a diameter of 3.75 cm (1.5"). Note that these cores were much longer than the 7 cm long cores in the earlier Xanthan experiments reported by [Langaas and Stavland, 2019]. Porosity of all three cores were measured to be 0.22 with an absolute permeability around 1 Darcy. Flooding experiments were performed with three different injection polymers, all following the same procedure. Fluid was injected with a Quizix QC pump (see Figure 3.3) and the differential pressure across the core was measured with a Fuji FOX series transmitter. The confining pressure was approximately 70 bar. The experimental set up is illustrated in Figure 3.5. Note that the core was placed in a vertical position during all core floods.

This part was more advanced and the following procedure was applied in this order;

1. The dry core was mounted into a core holder and filled with Alvheim formation water. Different parameters were measured (porosity, absolute permeability and pore size).

Figure 3.3: Quizix QC pump, used for injection during core flood experiments.

2. Oil was then injected and flooded to initial water saturation, Sw_i, in the opposite direction of flow shown in Figure 3.5. Marcol was injected first, which is a viscous oil with viscosity of 33 mPa·s, then a low viscosity oil, Isopar-H, was injected. The viscosity of Isopar-H is approximately 1 mPa·s. The reason for using the viscous oil was to get down to realistic values of Sw_i. The low viscous oil is more representative for Alvheim mobility ratio. Relative permeabilities and Sw_i were calculated based on flow rates and material balance measurements.

3. In the next step, Alvheim formation water was injected (flow direction as in Figure 3.5) to residual oil saturation, S_{or}. Water relative permeability and residual oil saturation were calculated based on measured flow rate and extracted volumes.

To this point all steps were completed at room temperature (20°C) for simplicity. To simulate Alvheim reservoir conditions, temperature was now increased to 70°C. Figure 3.4 shows the oven that was used in the core flood experiments at reservoir temperature.

Figure 3.4: Oven containing the core holder at 70 °C.

4. When brine flooding (continued from step 3) was stable at 70°C, seen by a stable differential pressure over the core, injection of polymer could start. In all injection steps, cumulative volume, differential pressure over core and injection rate were monitored.

   (a) Polymer was injected into the core. The polymer solutions were mixed as described in section 3.1.

   (b) Polymer was injected from a pressurized piston cell mounted outside the oven. To avoid injection of cold fluid, fluid was injected through a coil of 6-meter, placed in the oven, before entering the core. A spacer ring was mounted inside the core holder. This was to better control the formation of an external polymer filter cake; which shows to be an important detail [Langaas and Stavland, 2019]. Produced fluid from the core entered another cell outside the oven, with back pressure of 7 bar. More oil was produced during the polymer injection, and was used to calculate a new S_{or}. Corrected S_{or} is discussed further below.

   (c) In the beginning polymer was injected at constant flow rates; 2 ml/min, 1 ml/min and 0.5 ml/min. When the polymer front hit the core inlet, the pump mode was changed to constant pressure and polymer was injected at three different inlet pressures.

5. After polymer injection was finished, AFW was backflooded to stable conditions,

and RRF_w was measured. Then oil (Isopar-H) was backflooded and RRF_o was measured. Rate and differential pressure over core were monitored. Residual resistance factors, RRF_w and RRF_o, were compared. AFW was again backflooded as the last fluid through the core before the core was divided into four parts.

6. The core were then divided into four parts, each approximately 6 cm long, see Figures 3.6 and 3.7. AFW was backflooded for all four parts and individual RRF_w values were calculated. Figure 3.8, shows how the cores were mounted in the oven.

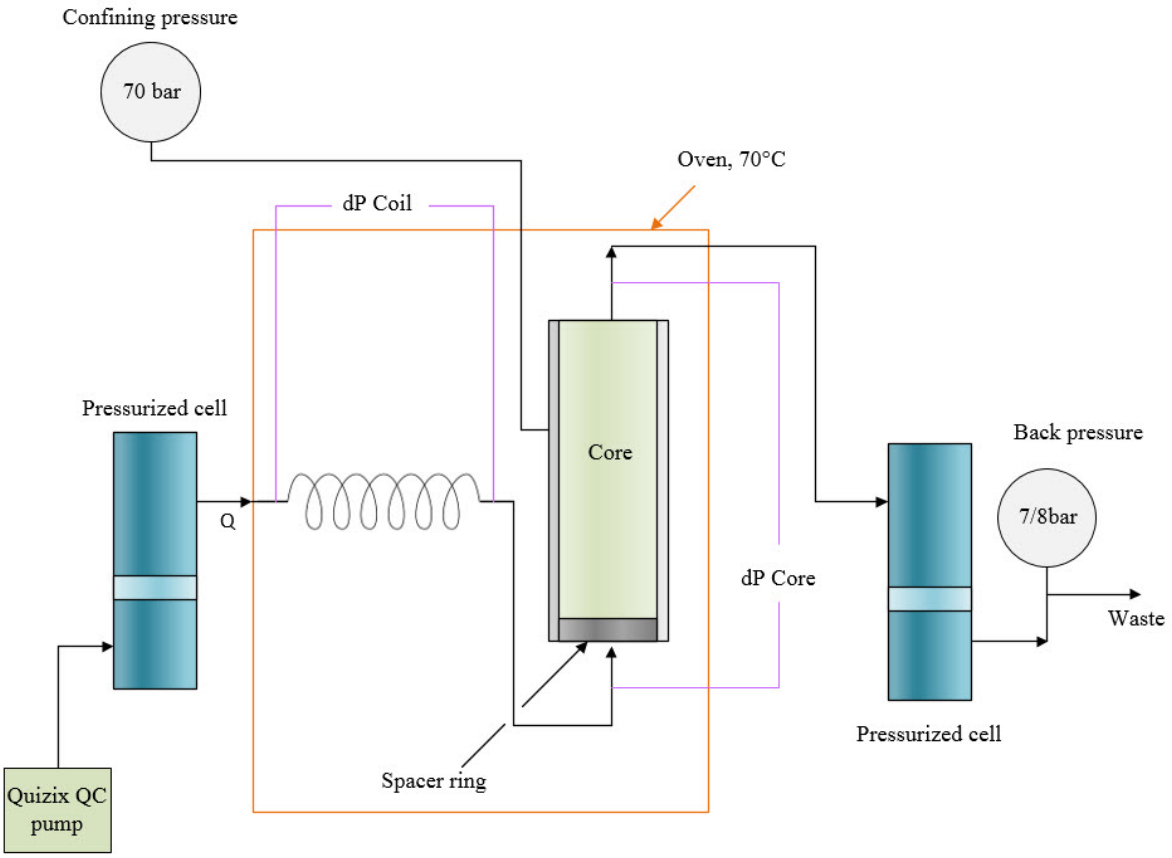

Figure 3.5: Experimental set up for polymer injection. Core holder was placed in the oven, connected to an inlet pressurized cell where polymer was injected and an outlet pressurized cell where polymer entered after flowing through core. Pressure transmitter outside the oven were connected to both the coil and the core that was placed inside the oven at 70°C.

Figure 3.6: Core divided in four parts

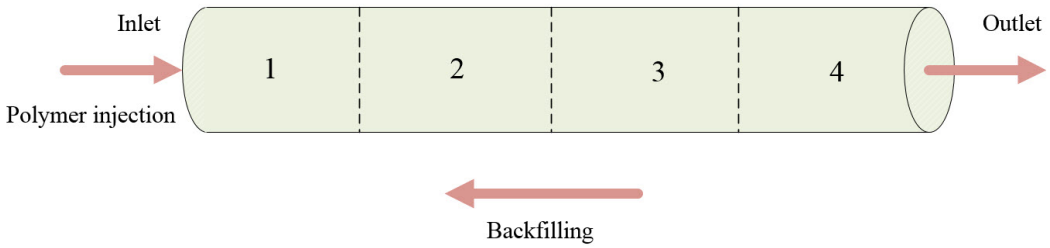

Figure 3.7: Description of core parts, where polymer was injected from left to right. Backflooding of AFW and Isopar were injected in opposite direction (from right to left). Cores were divided into four parts and AFW was backflooded from left to right for each part, as illustrated (1, 2, 3 and 4).

Figure 3.8: Vertical core (part 3) mounted in the oven. The coil is shown on the right side of the core.

Chapter 4

Results and discussion

4.1 Viscosity measurements

The results from viscosity measurements, measured with a rheometer (cone-plate), are shown for the different polymers. The bulk viscosities of all the polymers presented a shear-thinning behaviour and viscosity were matched with the Power-Law model, expressed in equation (2.17).

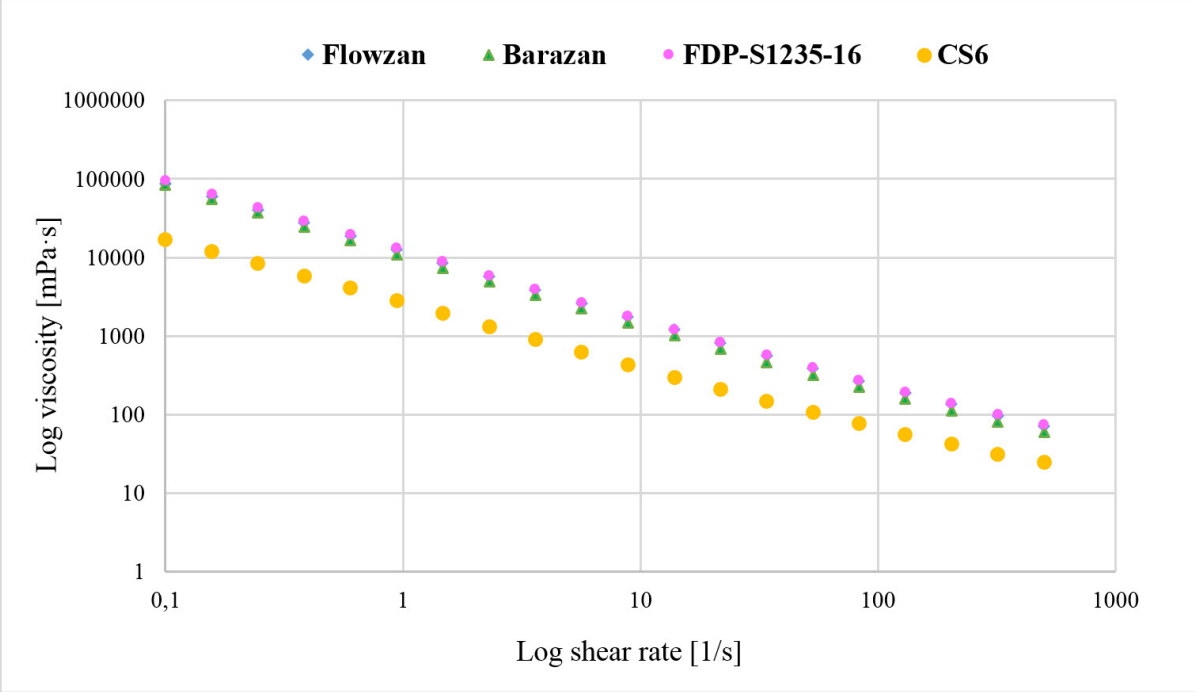

Figure 4.1: Viscosity behaviour of polymers for different shear rates, at 20°C.

Figure 4.1 include all polymers in one plot for comparison. Each polymer solution are also illustrated in Figures 4.2-4.5 below, to show that viscosity were matched with the Power-Law equation.

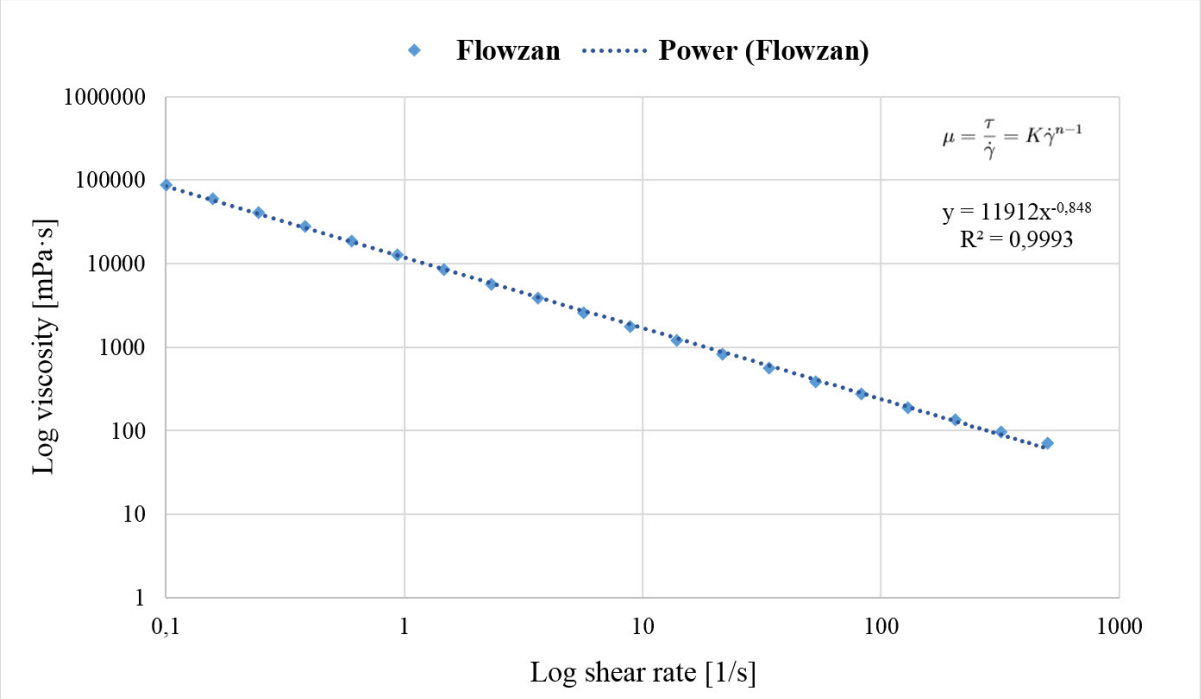

Figure 4.2: Viscosity of Xanthan (Flowzan) measured at 20°C.

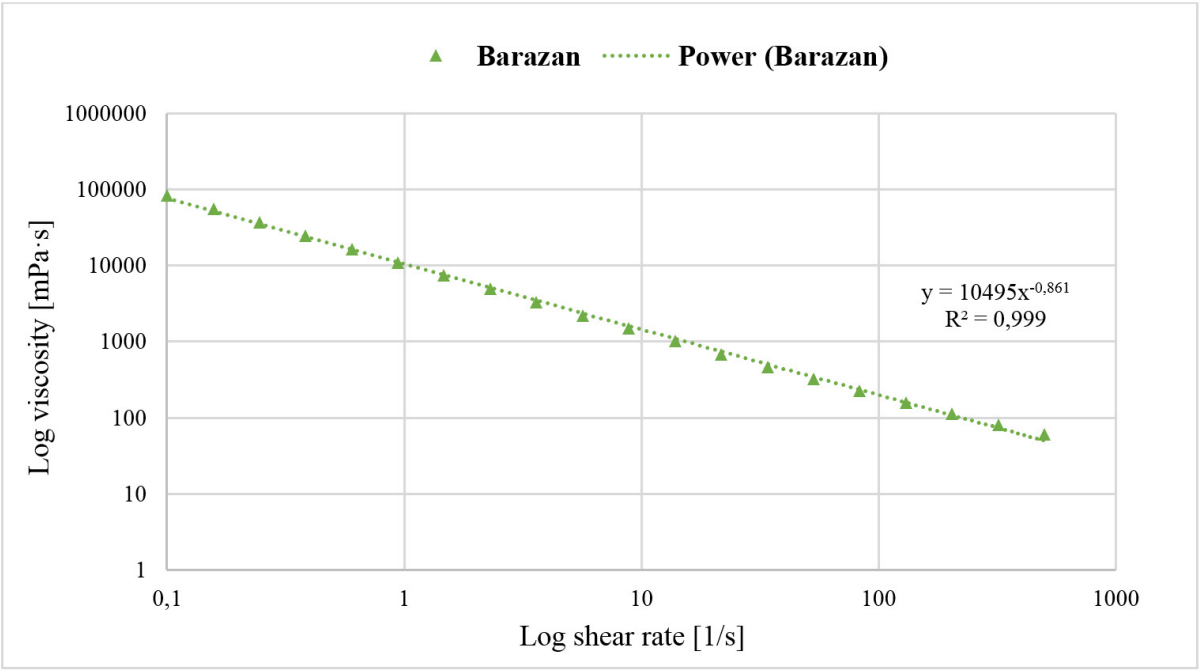

Figure 4.3: Viscosity of Xanthan (Barazan) measured at 20°C.

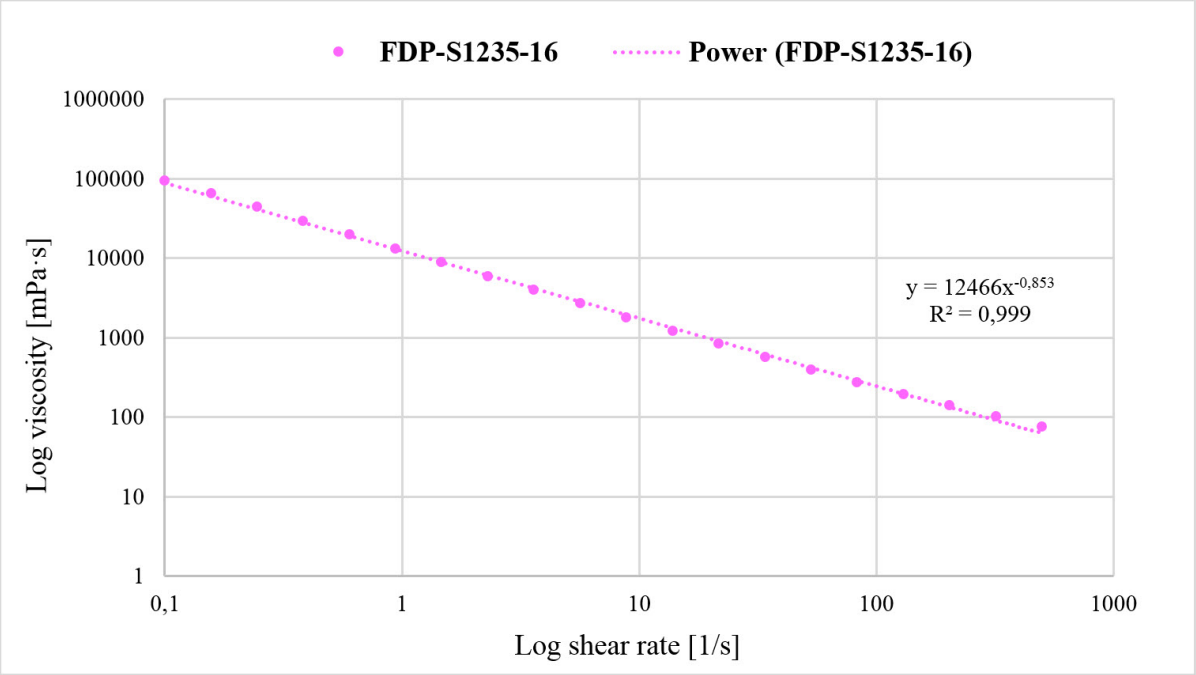

Figure 4.4: Viscosity of Xanthan (FDP-S1235-16) measured at 20°C.

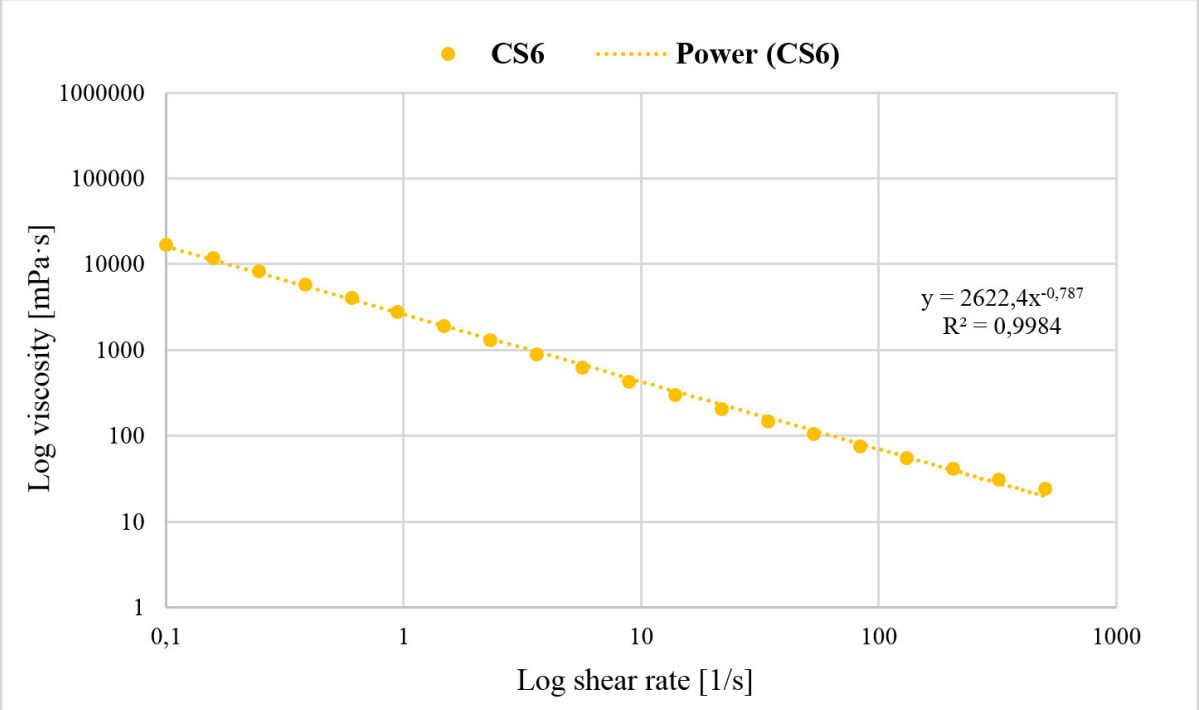

Figure 4.5: Viscosity of Scleroglucan, CS6, measured at 20°C.

Viscosity measurements have been performed on all polymer solutions that were mixed in this laboratory work.

4.2 Filter tests

4.2.1 Filtration tests at room temperature

Polymer solutions were filtered through different filter sizes with different pressures at a temperature around 20°C. Filter ratio, FR, was calculated and the results are presented in Table 4.1. Two different FR values are given, weight of 150 gram and 300 gram. See section 3.4 for a specific description of filter ratio calculation. Note that the symbol (-) is used for plugging of filter where 150 or 300 gram could not be measured. Two parallels were carried out for all filtration tests. Note that it is the average FR value that is presented in the table. Filter ratio values equal to 1 means no plugging of the filter. FR larger than 1 state a reduction in the flow velocity which indicate plugging of filter. As can be seen from Table 4.1, Scleroglulcan CS6 had poor filterability while Xanthan polymer FDP-S1235-16 indicated better filtration compared to both Flowzan and Barazan.

Table 4.1: Filtration tests at approximately 20°C

Polymer type	Pressure [bar]	Filter size [μm]	FR 300 gram	FR 150 gram
Flowzan	10	41	134.3	1.2
Barazan	10	41	0.9	1.2
FDP-S1235-16	10	41	1.2	1.1
CS6	10	41	-	-
Flowzan	20	20	1.3	1.0
Barazan	20	20	1.3	1.0
FDP-S1235-16	20	20	1.0	1.0
CS6	20	20	-	-
Flowzan	50	8	-	5.5
Barazan	50	8	-	47.7
FDP-S1235-16	50	8	6.8	2.0
CS6	50	8	-	-

Values that were used to calculate filter ratios are also illustrated in figures 4.6 - 4.8. Measured weight on y-axis is plotted against time on the x-axis.

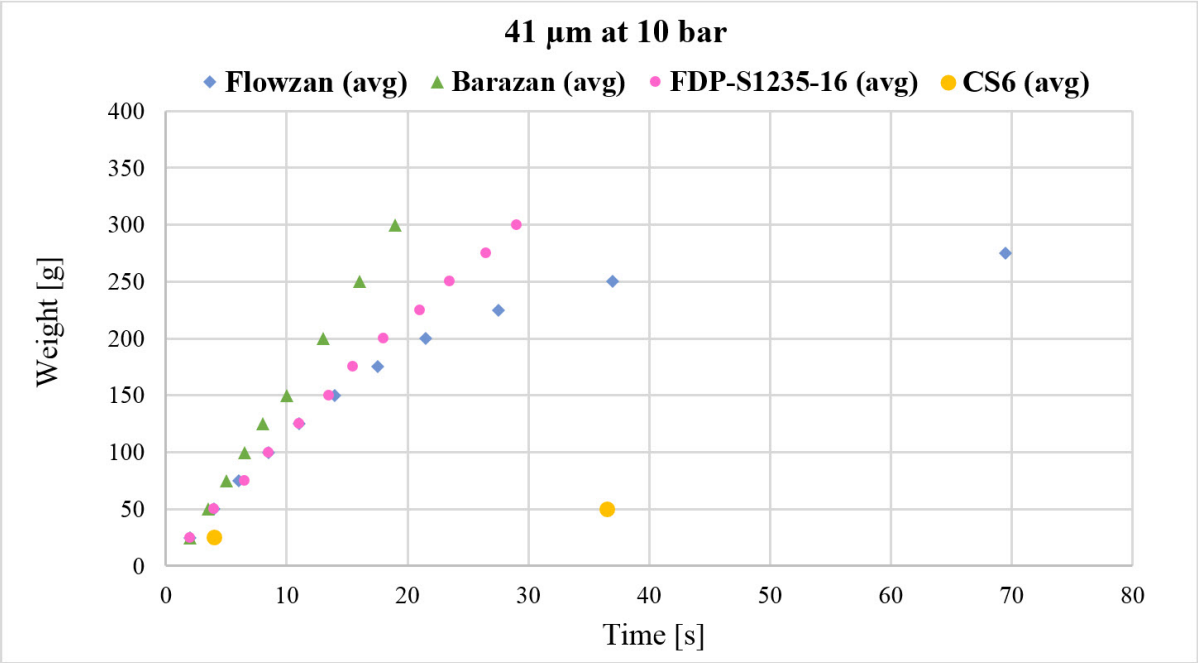

Figure 4.6: Filtration test with filter size 41 μm and 10 bar, at 20°C.

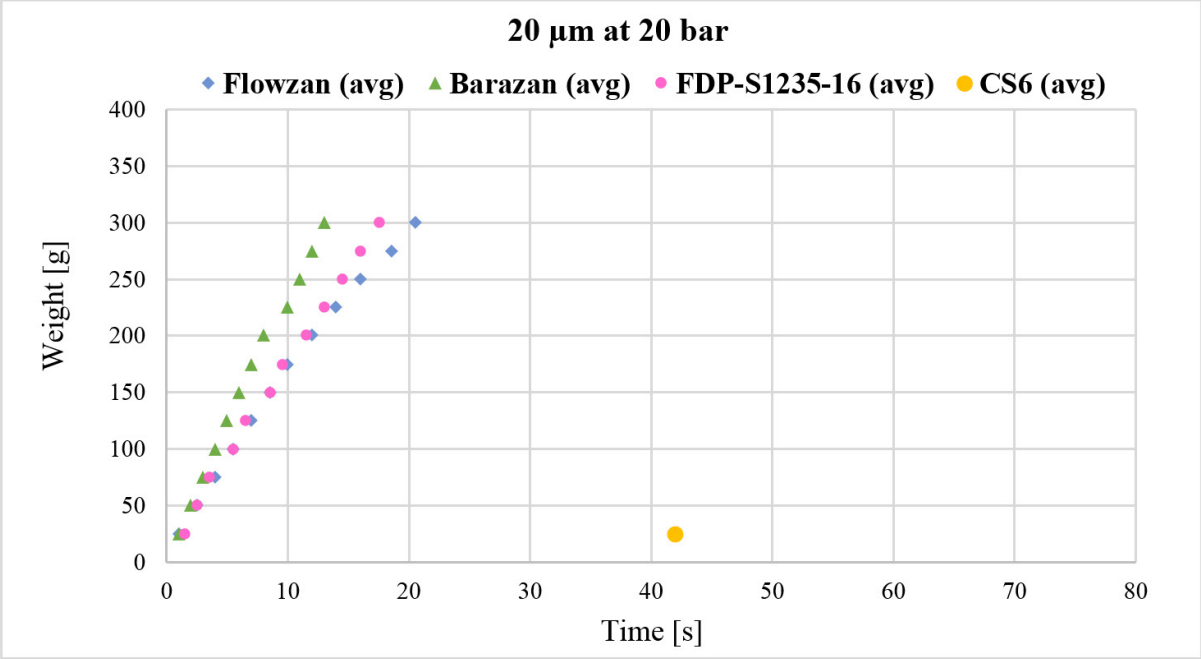

Figure 4.7: Filtration test with filter size 20 μm and 20 bar, at 20°C.

From these plots it clearly shows which of the polymers that have poor filterability through different filter sizes. If plugging appears, plotted values will deviates from a straight line. In Figure 4.8, seen from the early curve deviation of a straight line, it is shown that plugging appeared faster at 50 bar with filter size 8 μm, compared to slower filter plugging at 10 bar and 20 bar, shown in Figures 4.6 and 4.7.

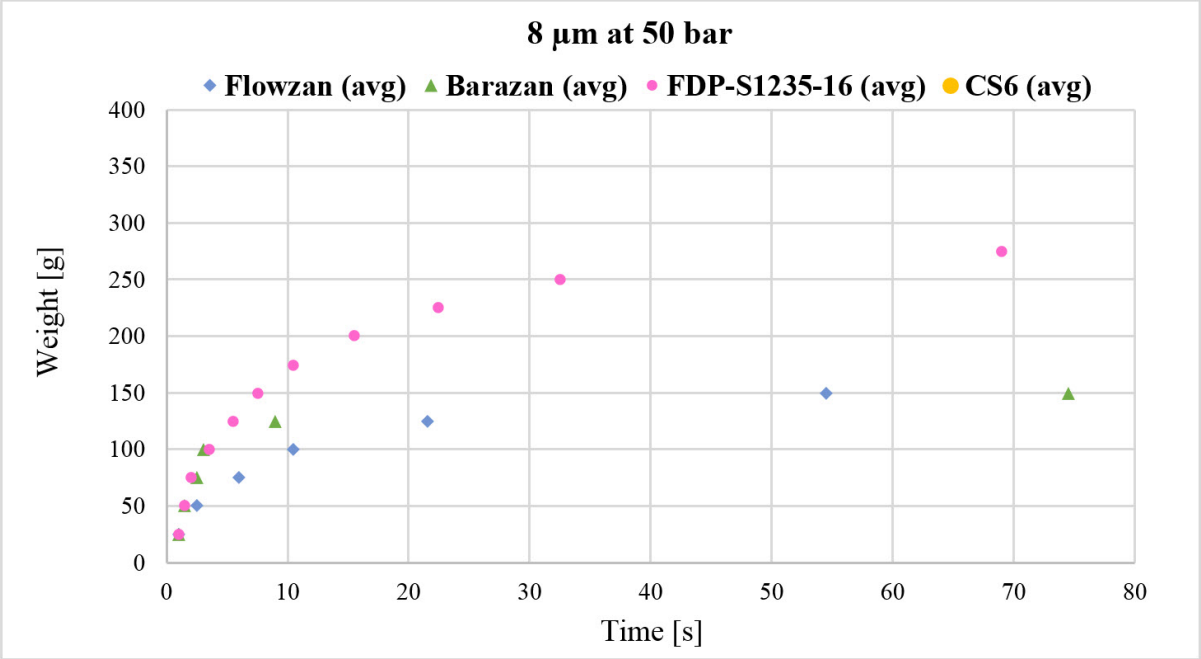

Figure 4.8: Filtration test with filter size 8 μm and 50 bar, at 20°C.

4.2.2 Filtration tests at reservoir condition

Filtration tests of Flowzan and CS6 were also performed at 70°C. This was necessary to understand how the polymer plugging behaviour could change with temperature. The plugging seen from earlier filtration tests of CS6 at room temperature, differs a lot from the same filtration tests at reservoir temperature, 70°C. The results are given in Table 4.2. For Flowzan, plugging was still observed from the measured filter ratio, also shown in Figure 4.9 where the plotted weight show a small deviation from a straight line. In Figures 4.9-4.10, both weight and flow rate on the y-axis are plotted against average time on the x-axis. Increasing flow rate with time indicate the opposite of plugging, seen in Figure 4.10. It is known that polymers have a temperature dependent viscosity, and hence, polymer plugging may vary with the change in temperature.

Table 4.2: Filtration tests at 70°C

Polymer type	Pressure [bar]	Filter size [μm]	FR 300 gram	FR 150 gram
Flowzan	50	8	1.3	1.0
CS6	50	8	0.6	0.8

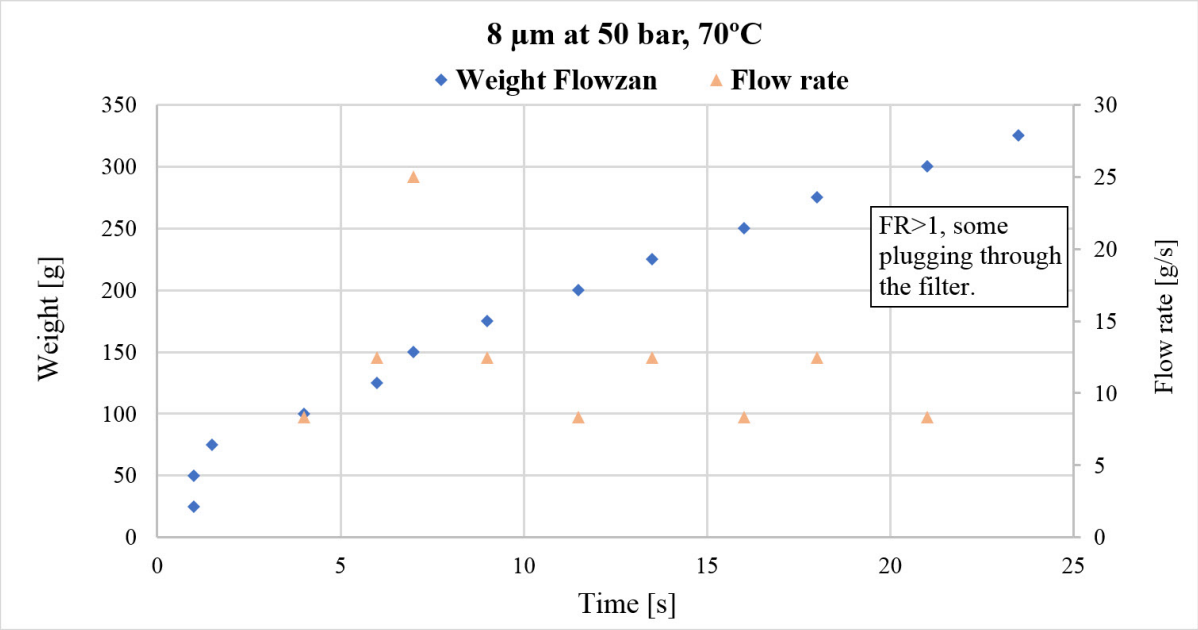

Figure 4.9: Filtration test for Flowzan with filter size 8 μm and 50 bar, at 70°C.

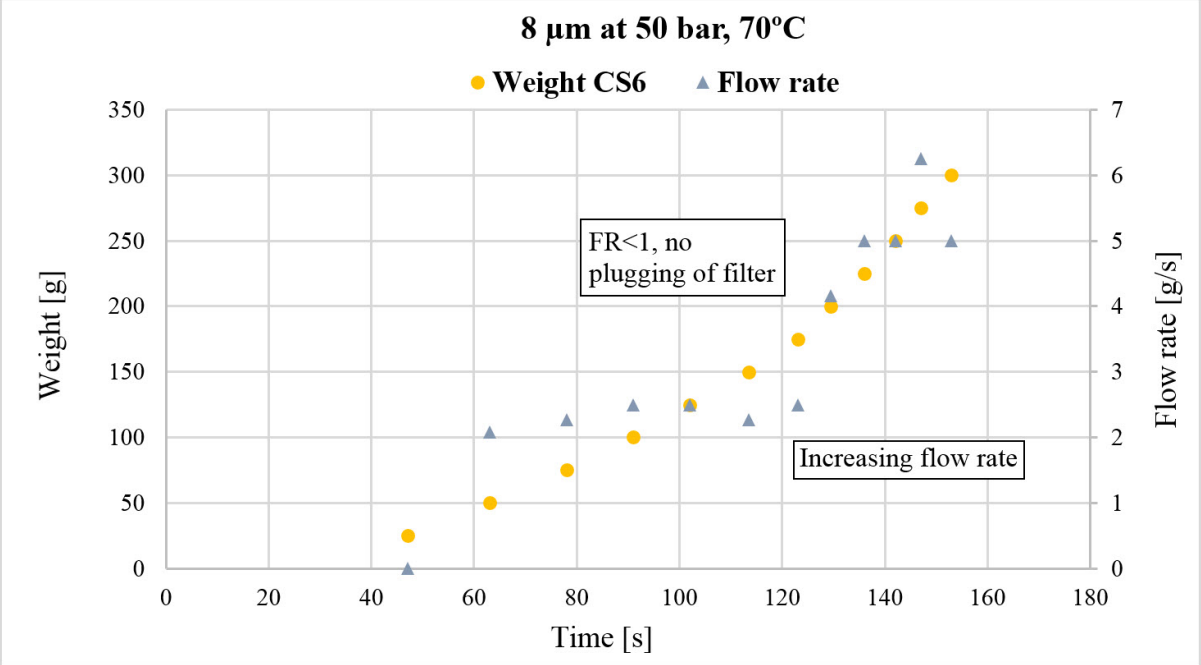

Figure 4.10: Filtration test for CS6 with filter size 8 μm and 50 bar, at 70°C.

4.3 Core flooding

Four core flooding experiments were performed with three different types of polymers. Polymers used in this part were based on results from earlier filtration tests. Flowzan, Barazan and CS6 were used because these polymers indicated poor filterability. The

procedure described in section 3.5 was followed as good as possible and deviations are explained when the related results are presented.

All cores were initially saturated with water, and both S_{wi} and S_{or} were measured with respectively oil and water flooding before polymer is injected. Saturation and permeability values can be seen in Table 4.3. Note that permeability is given in Darcy and K_o is the permeability for Ispoar. Pore size radius has been calculated from the given expression in Equation (2.15).

Table 4.3: Saturation and permeability values. All permeabilities are given in Darcy.

Polymer flood	K_{abs}	K_o	K_w	R_{pore} [μm]	S_{wi}	S_{or}	$NewS_{or}$
Flowzan	1.03	1.15	0.14	6	0.12	0.38	0.35
Barazan	1.00	1.17	0.09	6	0.10	0.45	0.43
CS6	1.10	0.74	0.12	6	0.14	0.40	0.31

Note that when S_{wi} for Barazan should be measured, some of the collected water from the separator was lost. It was tried to measure the lost volume and it has been corrected for.

4.3.1 Core flood experiment with Flowzan

Flowzan was initially injected with constant rate of 2 ml/min before changing to constant differential pressure (DP core). DP core was set to 10 bar, and changed to 29 bar after approximately 2 hours of flooding. Note that this injection method was not following the procedure; in this case differential pressure was set to constant instead of constant inlet pressure. Injection rate, inlet pressure and differential pressure were all monitored during polymer injection. These parameters are given in Figures 4.11 and 4.12, where injection rate and pressure on the y-axis are plotted against injection time on the x-axis. A flow rate (Calculated Q) calculated from measured volume and time during injection is used in the figures.

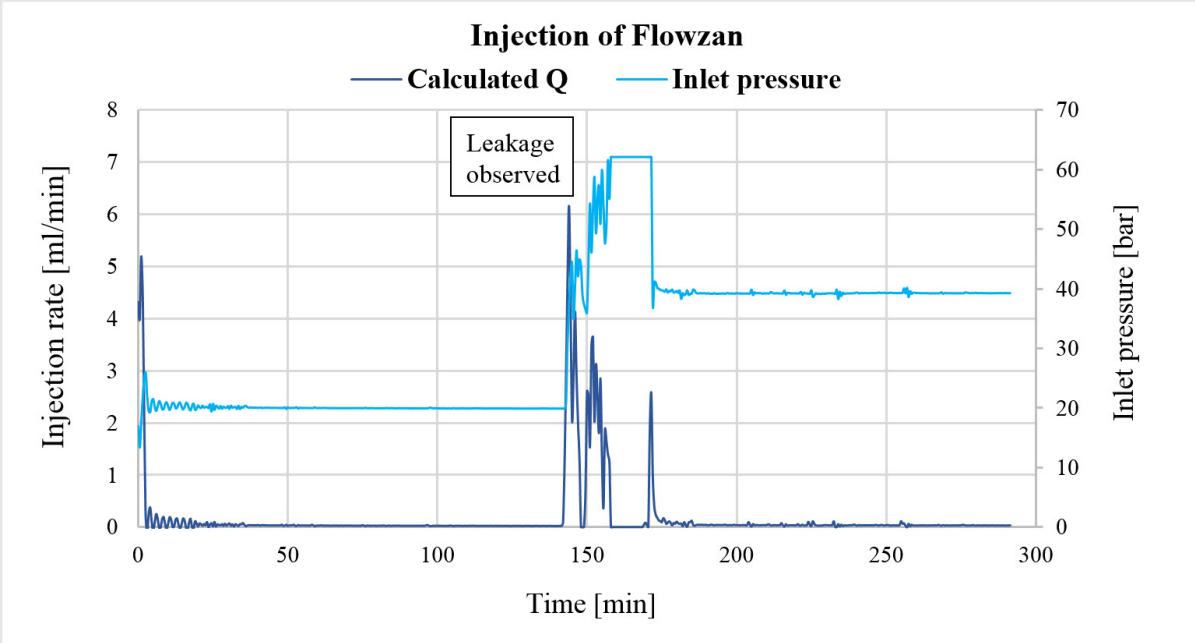

Figure 4.11: Inlet pressure and injection rate vs. time of injection, Flowzan

A back pressure of 8 bar was used. Note that the confining pressure was 50 bar when the differential pressure was set to 10 bar, then it was increased to 70 bar approximately after 150 seconds of injection. At this point the inlet pressure started to increase, hence, it was necessary to increase the confining pressure to not get erroneous flow between core and core holder. During this pressure increase, a small leakage of polymer was observed from the tubing. This leakage explains the behaviour of the injection rate and the inlet pressure parameters in Figure 4.11, at a time between 148-170 minutes. All tubing in the oven were changed from teflon tubing to another tubing of nylon, then polymer injection was continued with a confining pressure of 70 bar and at a differential pressure of 29 bar.

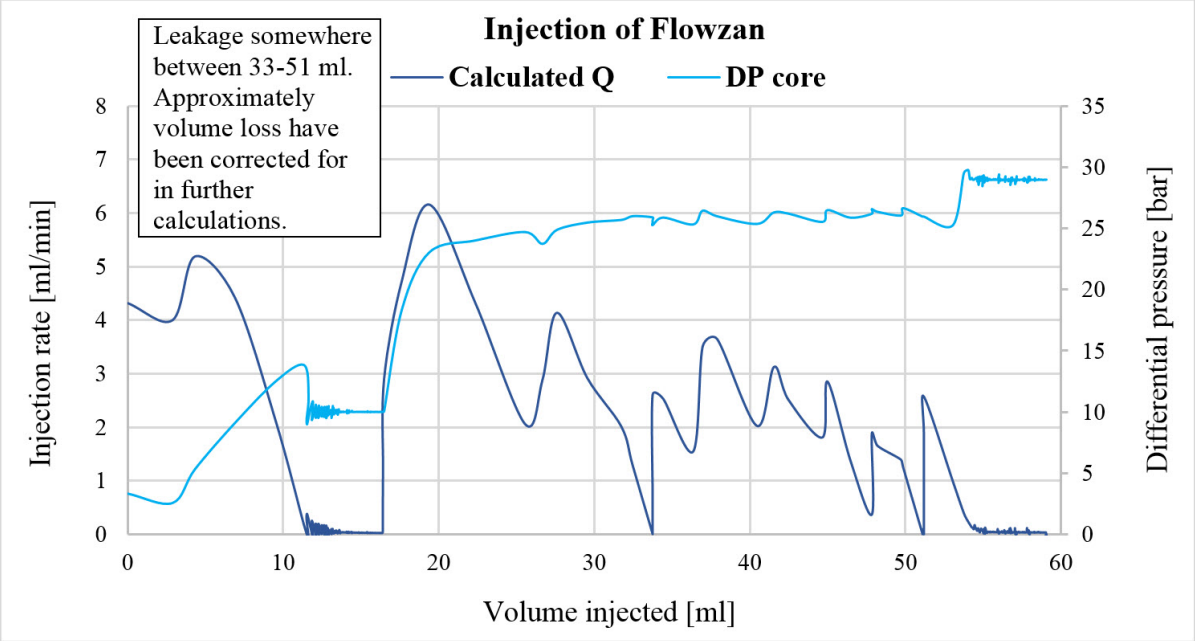

Figure 4.12: Constant dP and injection rate vs. volume injected, Flowzan

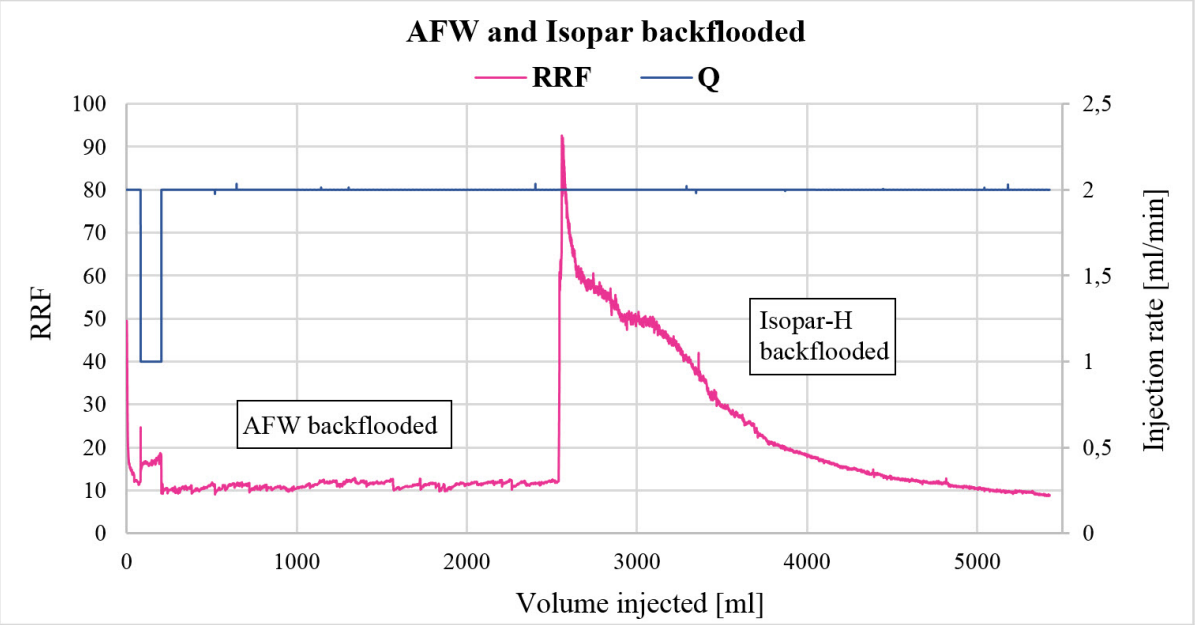

Figure 4.13: Residual resistance factor for AFW and Isopar vs. time, Flowzan

After a shut-in period of 3 days, AFW and Isopar were backflooded. After a backflood of 2540 ml (approximately 42 PV) AFW, 2885 ml (approximately 48 PV) Isopar was backflooded. It was observed that RRF_w stabilized around 12, while RRF_o decreased with injected volume and had a value of 8 when 48 PV was backflooded. When the experiment was ended, the value of RRF_o was still decreasing, and hence the productivity of oil was increasing with volume of flooded oil. Both AFW and Isopar were backflooded

with constant rate, 2 ml/min, this is shown in Figure 4.13 together with values of RRF. Equation (2.25) has been used for calculation of RRF values.

Second injection with Flowzan

Since a leakage of polymer was observed in the Flowzan core flooding, it was difficult to know the exact amount of injected pore volume. This uncertainty initiated a new core flooding of Flowzan in the exactly same core. AFW was first backflooded again for 4 days before a new mix with Flowzan was injected.

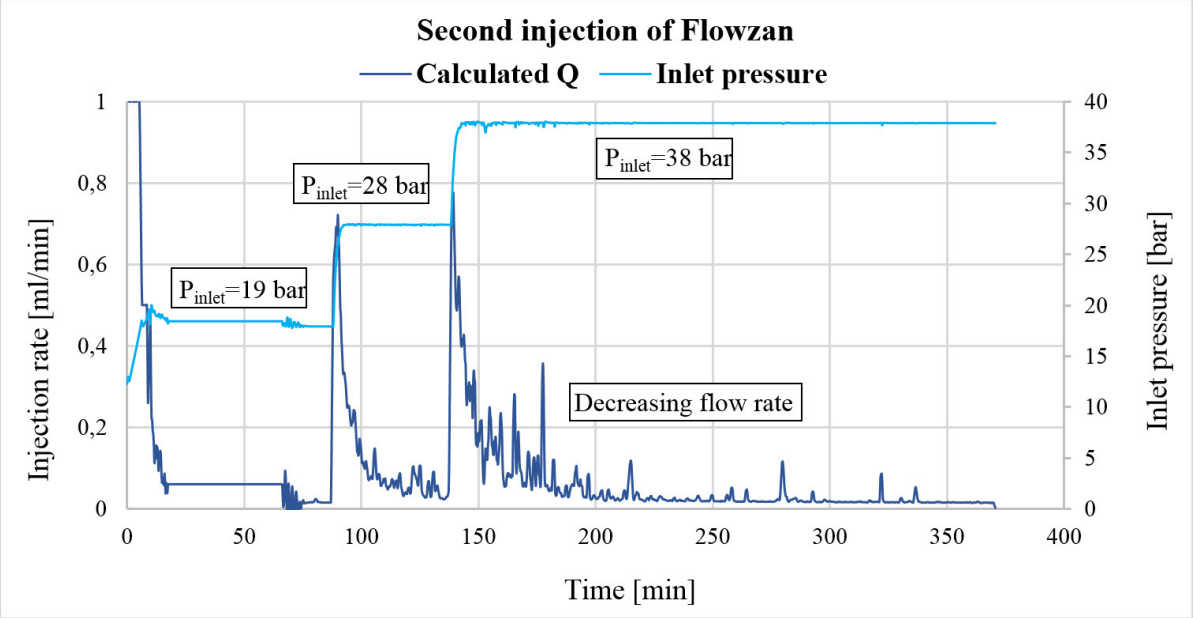

Figure 4.14: Inlet pressure and injection rate vs. time for second injection of Flowzan.

Before polymer injection it was assumed that the core was flooded to initial S_{or} (0.38). Note that injection method for this experiment was changed to constant inlet pressure mode, as described in the procedure, instead of constant differential pressure mode. Results are shown in Figure 4.14, where injection rate and inlet pressure on the y-axis are plotted against time on the x-axis. In Figure 4.15, injection rate and the differential pressure on the y-axis are plotted against volume on the x-axis. From this figure (Figure 4.15) it can be seen that the differential pressure was almost stabilized before the inlet pressure was changed to a higher value.

Three different inlet pressures were applied (19, 28 and 38 bar) and 32 ml (0.5 PV) of Flowzan was injected. For every change in inlet pressure it was observed that injection rate was decreasing, see Figure 4.14. Decreased injection rate may indicate plugging of polymer in the core. Mobility reduction, also called resistance factor (RF), is plotted in Figure 4.16.

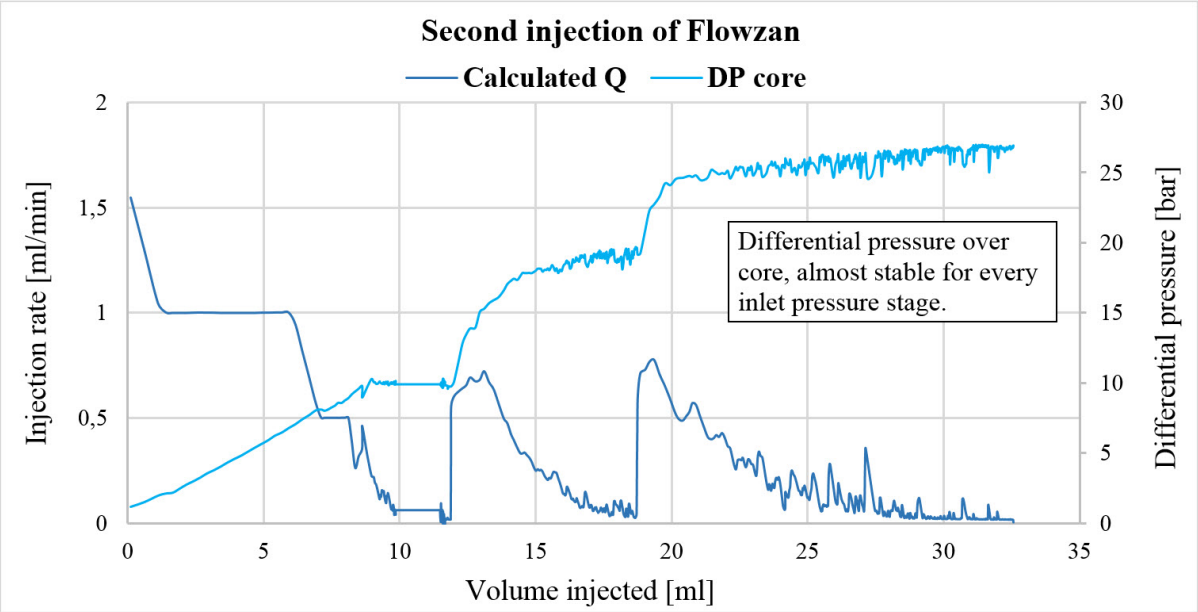

Figure 4.15: Constant differential pressure and injection rate vs. volume injected for second injection of Flowzan.

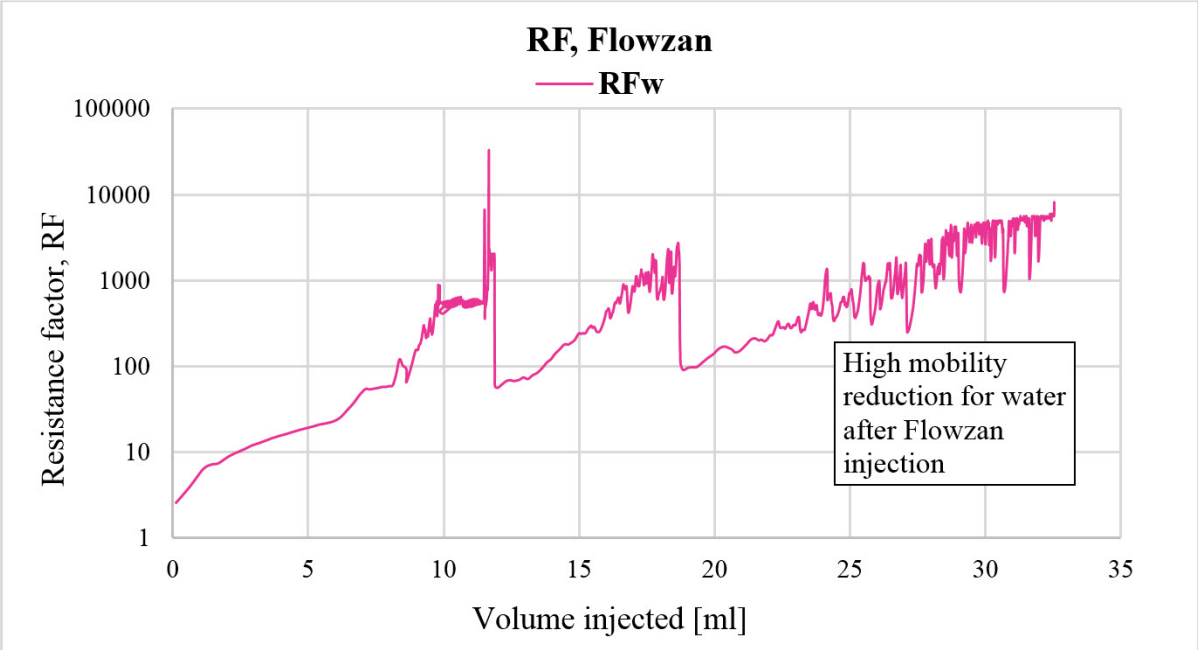

Figure 4.16: Resistance factor with Flowzan after second injection.

For this core flood, only AFW was backflooded and RRF_w was stable on a value around 23. Note that this was a higher reduction in water permeability, compared with the previous attempt. See Figure 4.17.

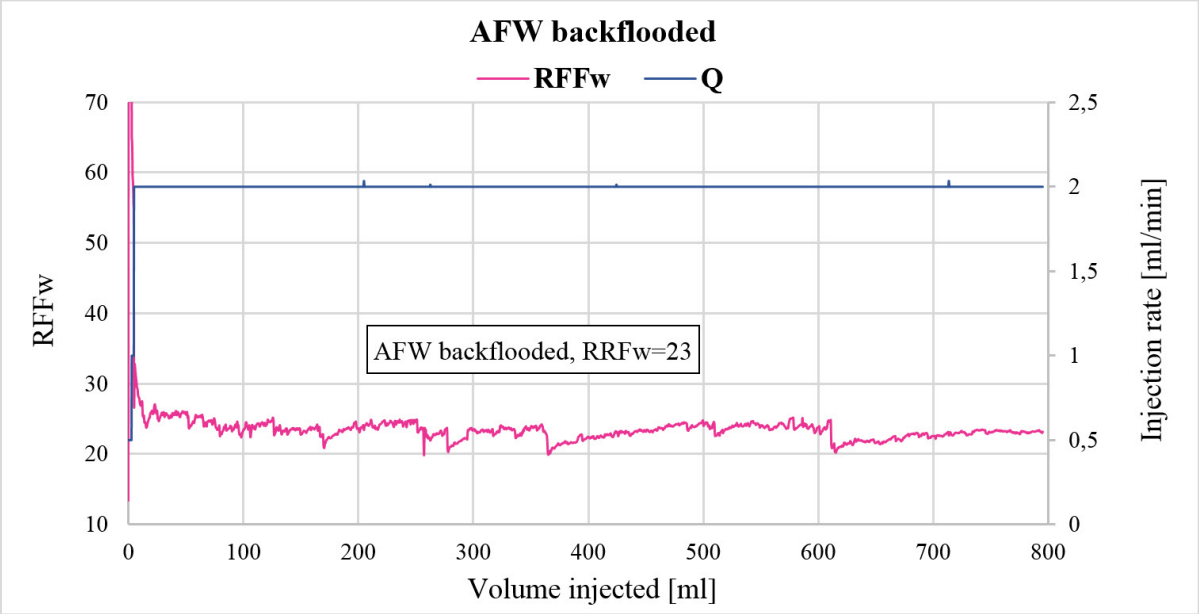

Figure 4.17: Residual resistance factor for AFW vs. time when AFW was flooded back.

The flooded core was divided into four segments and each of these parts were separately backflooded with AFW. Results are shown in Table 4.4. Calculation of permeability and residual resistance factor are described in section 2.1.1.

From Table 4.4 it is easily shown that reduction in water permeability mainly occurred at the inlet part of the total core, part 1. It is important to mention that a filter cake was observed at core inlet. This filter cake was removed before the core was divided. Equation (2.5) have been used to calculate the residual resistance factor for part 1 with filter cake attached, and a new value was given, $RRF_{w,1} = 90.3$.

Table 4.4: Results after backflooding for all four parts.

Core part	Length [cm]	$K_{w,i}$ [mD]	$RRF_{w,i}$
Part 1	5.95	4	34.1
Part 2	6.02	155	0.9
Part 3	6.10	100	1.4
Part 4	6.21	118	1.2

Average RRF for the four parts, RRF_{avg}, is given in table 4.6.

4.3.2 Core flood experiment with Barazan

In another core flood experiment, Barazan was injected. The different constant inlet pressures were 15, 25 and 35 bar respectively. Every pressure step had a duration of 1 hour. Back pressure was 7 bar and confining pressure set to 70 bar.

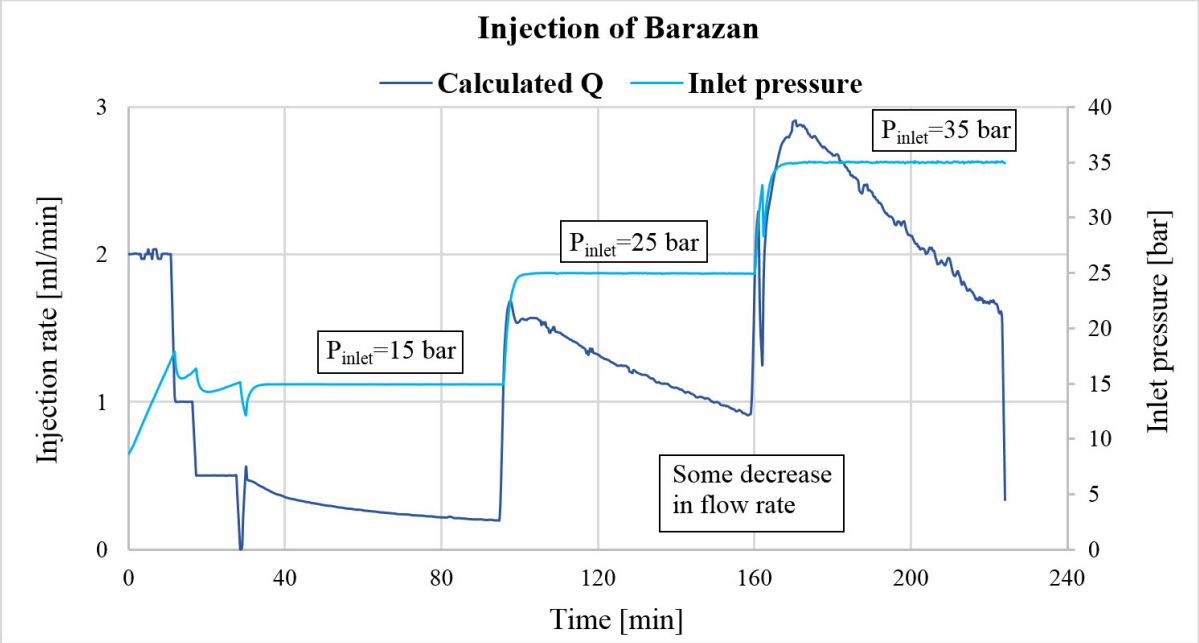

Figure 4.18: Inlet pressure and injection rate vs. time for injection of Barazan.

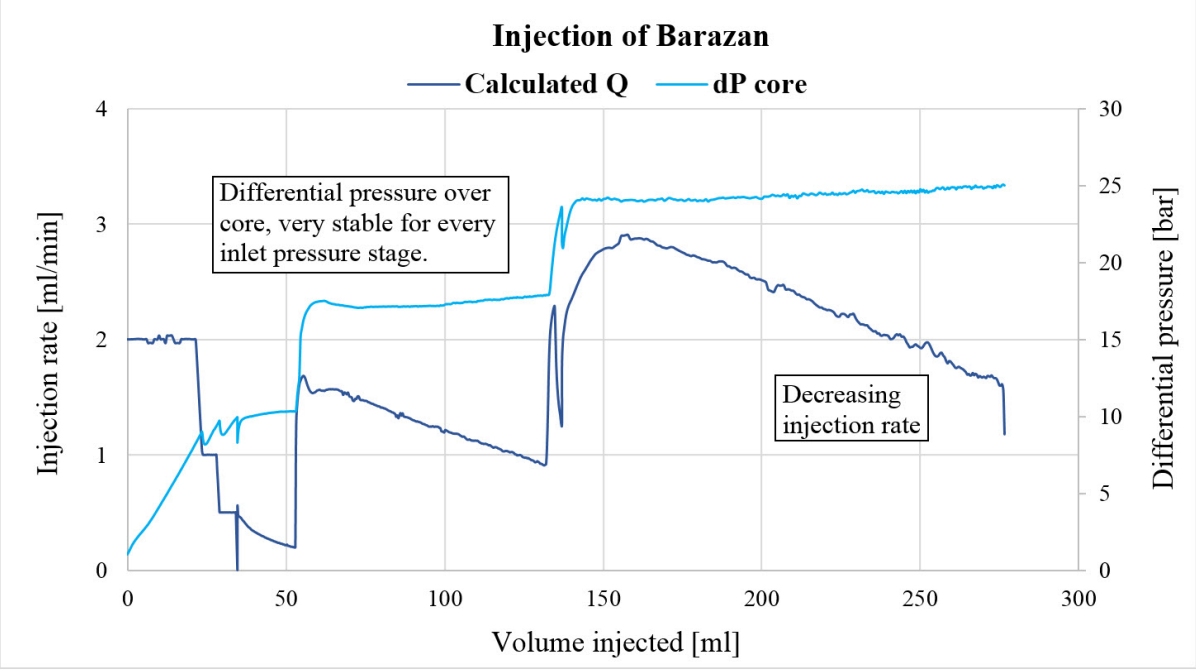

Figure 4.19: Constant differential pressure and injection rate vs. volume injected.

Results are presented in Figures 4.18 - 4.21. From Figure 4.18, it is observed that injection rate (on y-axis) decreases with time (on the x-axis) for all the different inlet pressures. This is also seen in Figure 4.19, where it also shows that the differential pressure (on y-axis) was almost stabilized when inlet pressure was changed. The decreased flow rate may indicate that the polymer was plugging in the core. In total 277.5 ml (4.5 PV) of polymer was injected.

Resistance factor, RF, is illustrated in Figure 4.20. This water phase mobility reduction, was much lower than compared with the same mobility reduction for Flowzan.

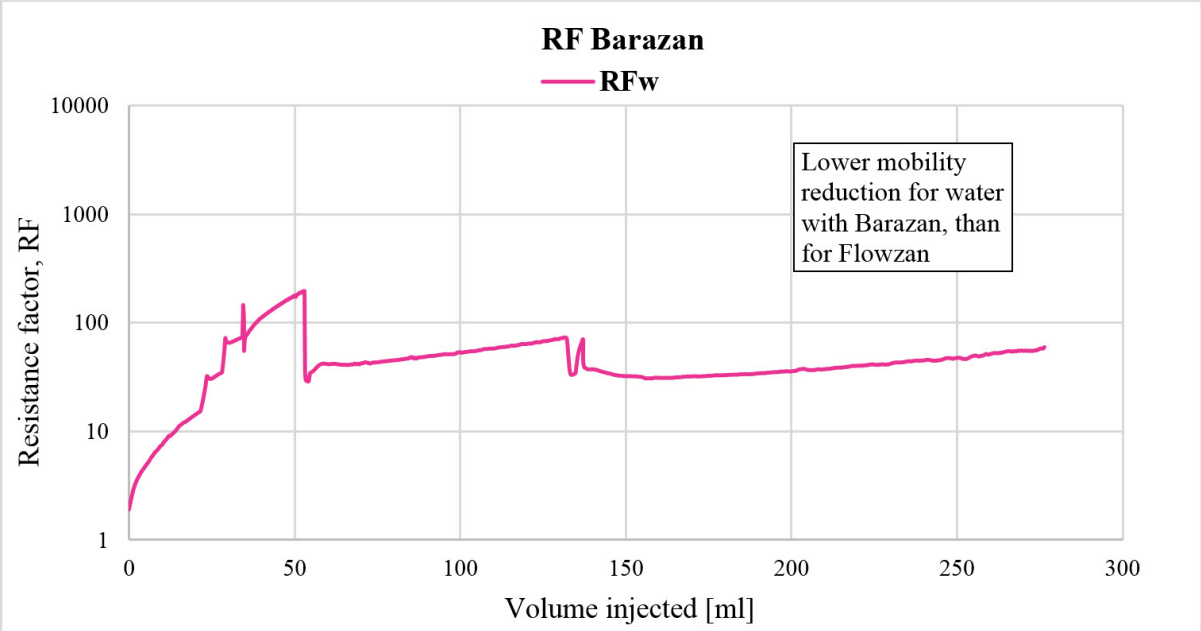

Figure 4.20: Resistance factor with Barazan.

After a shut-in period of 5 days, AFW and Isopar were backflooded. 2527 ml (approximately 40 PV) AFW and 2847 ml (approximately 48 PV) Isopar were flooded. RRF_w was slightly increasing, while RRF_o was decreasing with volume injected. This is illustrated in Figure 4.21. From this figure it clearly shows the change in RRF from AFW to Isopar. Both AFW and Isopar were backflooded with constant rate, 2 ml/min. The value of RRF_o after this polymer flood was very high compared to the same value from Flowzan polymer flooding, even though it would continued to decrease with more volume injected. This can be related to poor plugging of Barazan in the core compared to Flowzan.

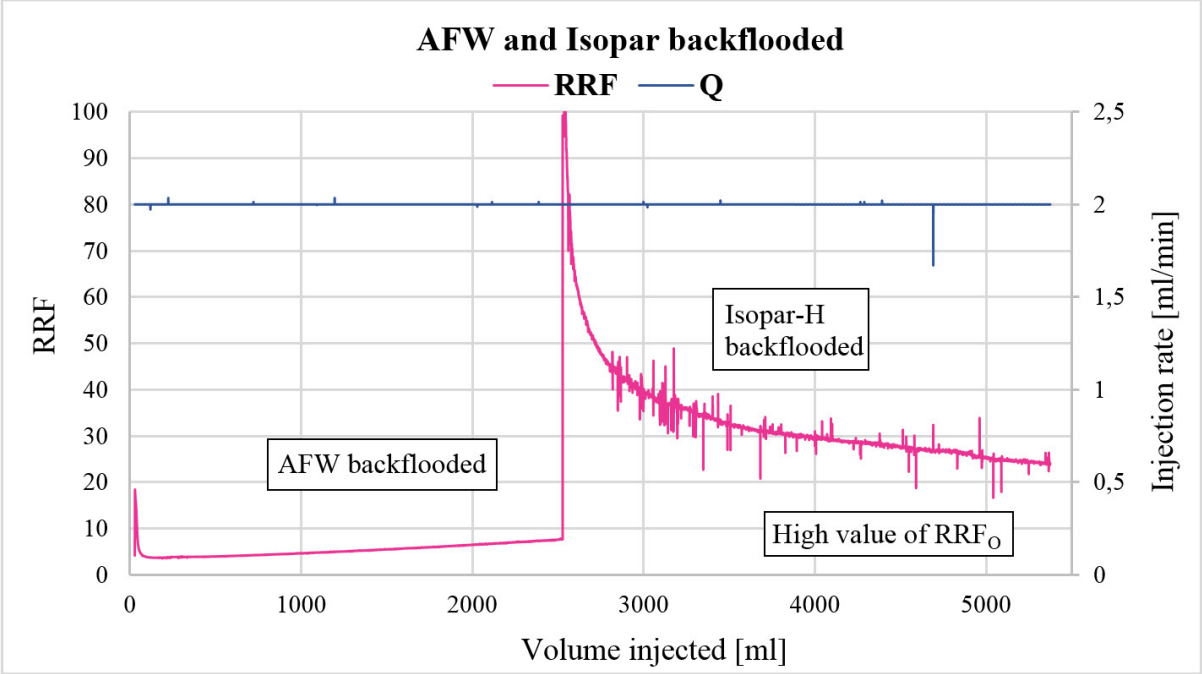

Figure 4.21: Residual resistance factor for AFW and Isopar vs. time.

After polymer injecion and backflooding, the core was divided into four parts and each of these parts were separately backflooded with AFW. Results are shown in Table 4.5. From these results it were observed that part 1 have the lowest water phase permeability, and hence, highest value of RRF. From this polymer injection there was only observed a small filter cake. For core inlet, part 1, a new value of RRF was calculated, $RRF_{w,1}$=24, when filter cake was attached.

Table 4.5: Results after backflooding for all four parts.

Core part	Length [cm]	$K_{w,i}$ [mD]	$RRF_{w,i}$
Part 1	6.10	15	5.9
Part 2	6.10	39	2.3
Part 3	5.90	51	1.7
Part 4	5.95	60	1.5

Average value of RRF for all the four parts is given in table 4.8.

4.3.3 Core flood experiment with Scleroglugan, CS6

Scleroglucan, CS6, was injected following steps given in the procedure. When polymer front hit the core inlet at approximately 22 ml of injected polymer, inlet pressure was changed to 19.5, 29.5 and 39.5 bar respectively.

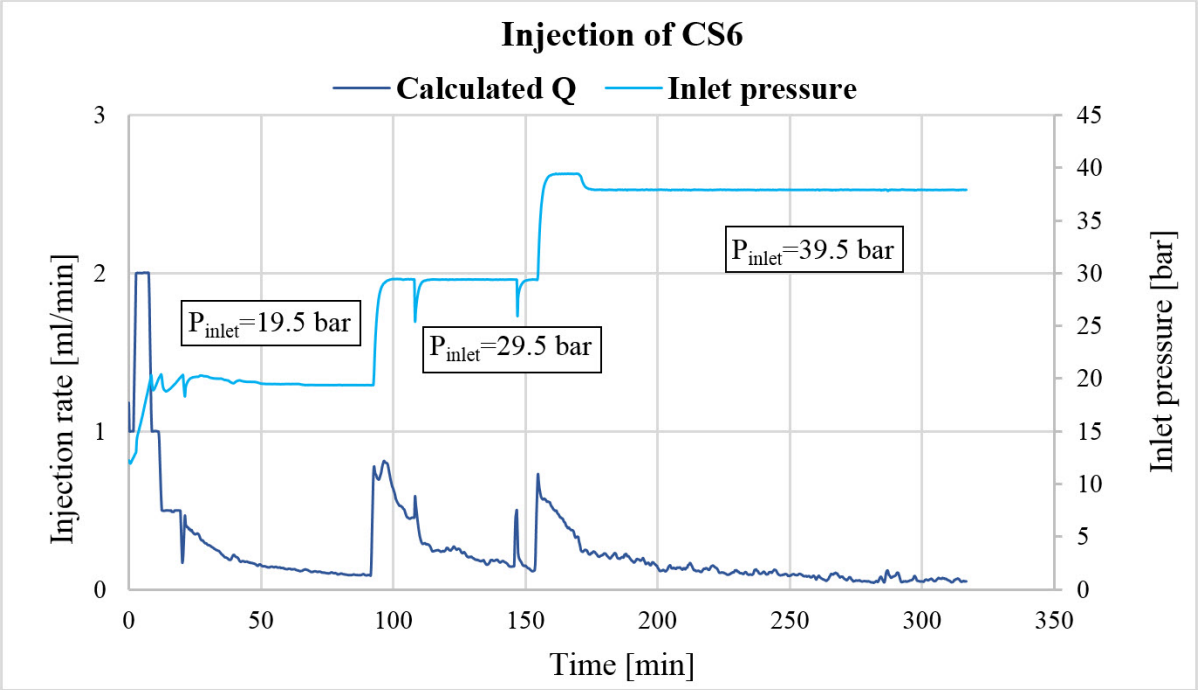

Figure 4.22: Inlet pressure and injection rate vs. time for injection of CS6.

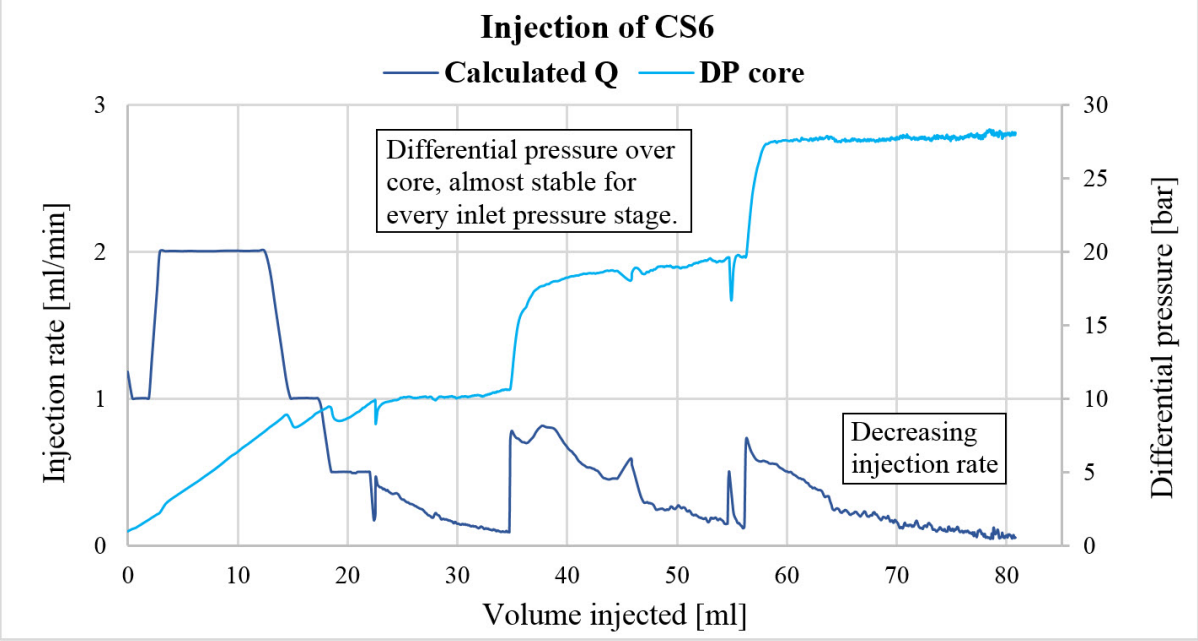

Figure 4.23: Constant differential pressure and injection rate vs. volume injected.

Figure 4.22 and 4.23 (where injection rate and pressures on the y-axis are plotted against time and volume, respectively, on the x-axis) shows that flow rate was decreasing for each step of increased inlet pressure.

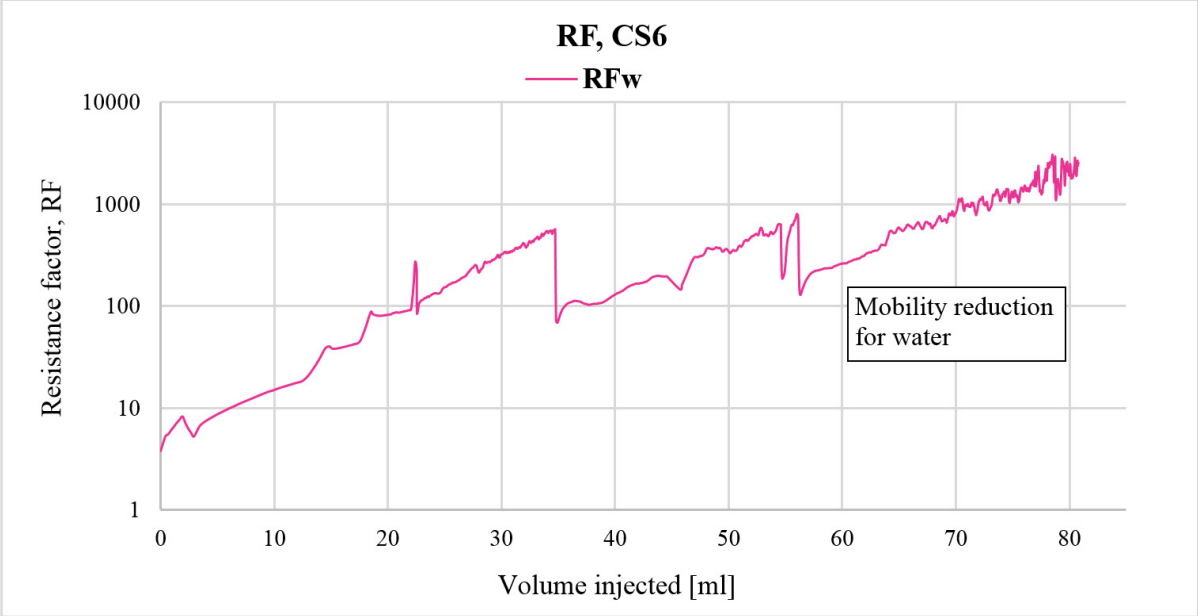

Figure 4.24: Resistance factor with CS6.

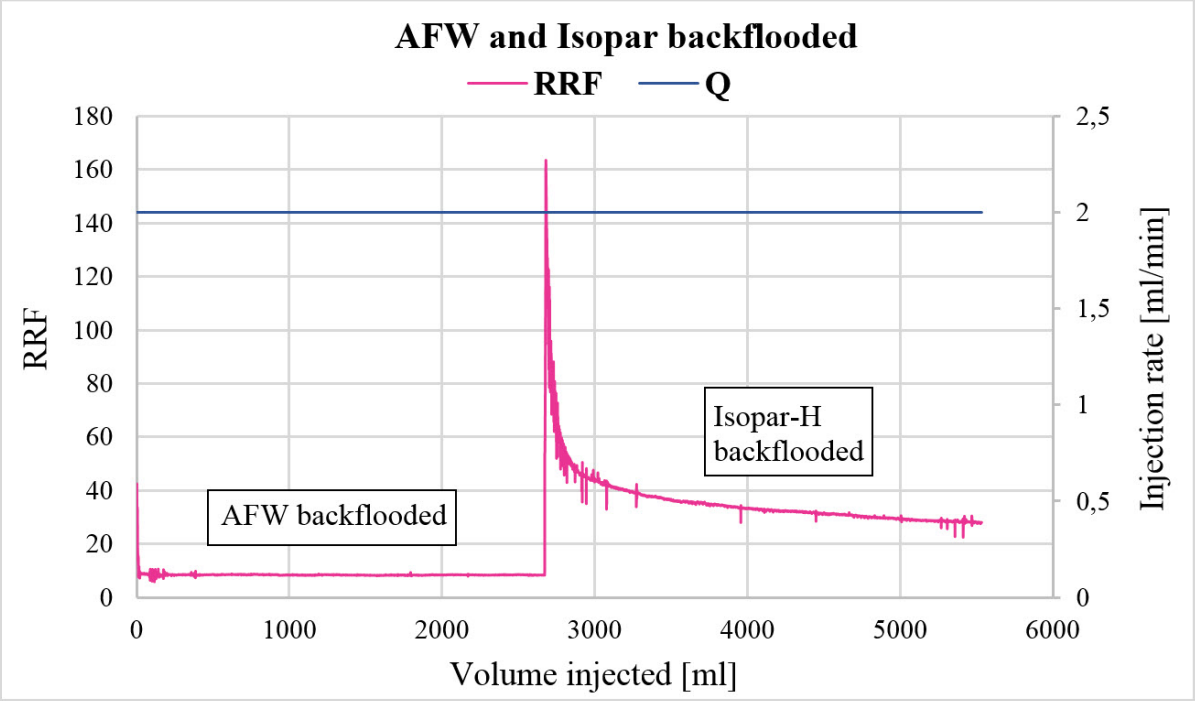

Figure 4.25: CS6 residual resistance factor for AFW and Isopar vs. time.

Both AFW and Isopar were backflooded. 2700 ml (approximately 45 PV) AFW and 2800 ml Isopar were flooded. RRF_w was stable at a value of 8, while RRF_o was decreasing with volume injected. This is illustrated in Figure 4.25. Even though RRF_o was decreasing, a high value was observed when the experiment was ended (RRF_o=27 at 5500 ml). Both AFW and Isopar were backflooded with constant rate, 2 ml/min.

Since RRF_o was higher than the earlier experiments, and RRF_w values low compared to injection with Flowzan, this core was not divided into parts.

4.3.4 Summarized results from core flooding experiments

The key results are summarized below to easier compare the polymer effect. Xanthan FDP-S1235-16 polymer was not used in core flood experiments because this polymer indicated lowest plugging through filter size 8 μm.

Table 4.6: Summarized results from Flowzan core flooding. Note that the symbol, (2), means value after second time of Flowzan injection.

Measured parameter	Value
Initial water permeability, K_w [mD]	140
End point water permeability, K_w [mD]	12
End point water permeability (2), K_w [mD]	6
Initial oil permeability, K_o [mD]	1150
End point oil permeability, K_o [mD]	130
RRF_w core	12
RRF_o core	8
RRF_w core (2)	23
Core divided into four parts	
$RRF_{w,1}$	34.1
$RRF_{w,2}$	0.9
$RRF_{w,3}$	1.4
$RRF_{w,4}$	1.2
$RRF_{w,avg}$	9.3
With filter cake $RRF_{w,1}$	90.3

Table 4.7: Summarized results from CS6 core flooding

Measured parameter	Value
Initial water permeability, K_w [mD]	120
End point water permeability, K_w [mD]	14
Initial oil permeability, K_o [mD]	740
End point oil permeability, K_o [mD]	26
RRF_w core	8
RRF_o core	28

Table 4.8: Summarized results from Barazan core flooding

Measured parameter	Value
Initial water permeability, K_w [mD]	90
End point water permeability, K_w [mD]	11
Initial oil permeability, K_o [mD]	1170
End point oil permeability, K_w [mD]	48
RRF_w core	7.5
RRF_o core	24
Core divided into four parts	
$RRF_{w,1}$	5.8
$RRF_{w,2}$	2.3
$RRF_{w,3}$	1.7
$RRF_{w,4}$	1.5
$RRF_{w,avg}$	2.8
With filter cake $RRF_{w,1}$	24.0

4.4 Discussion

Polymer properties have been evaluated for disproportionate permeability reduction as a method for water shut-off. Different biopolymers Xanthan and Scleroglucan have been used. First, filterability of these polymers were tested, depending on these results, DPR parameters were analyzed from core flood experiments.

The following parameters were measured:

- Viscosity, μ, for polymer solutions where shear-thinning Power-Law was matched at 20 °C (Equation (2.17)).
- Filter ratio, FR, was measured and analyzed from filter tests. FR>1 indicates plugging of the porous filter, and flow velocity will decrease. Plugging was observed for all different filter sizes.
- Residual resistance factor, RRF, for both oil and water. RRF values varied for each polymer but similar for all core floods was an almost stable RRF_w value and a decreasing value of RRF_o, when the experiment was ended.
- Resistance factor for water flow, RF_w. See table 4.9 for exact measurements.

In Table 4.9, shear rates were calculated by using Equation (2.21), where α was assumed to be 2.5. The apparent viscosity was then calculated from Equation (2.27). For polymer

Table 4.9: Results of resistance factor and parameters used for calculation of polymer permeability, k_p

Polymer	k_w [D]	RF_w	ΔP_p [bar]	q_p [ml/min]	$\dot{\gamma}_p$ [s^{-1}]	μ_{app} [mPa·s]	k_p [D]
Flowzan	0.14	9816	27	0.015	1.7	4582	0.096
Barazan	0.09	54	25	1.600	183.7	70	0.171
CS6	0.12	2212	28	0.059	6.4	364	0.029

permeability, k_p, at the end of polymer injection, Darcy Law was used (Equation (2.1)), and values of RF were calculated by using Equation (2.26). If there was no plugging in the core, then RF should be the same as the polymer viscosity, μ_p. For Flowzan, RF was larger than μ_p with a factor of 2.1. This means that there had to be an additional effect, e.g, plugging, that caused this higher value of RF. The same effect was shown for CS6. RF was larger than μ_p with a factor of 6. From these observations, both Flowzan and CS6, indicate plugging in the cores. Barazan was injected at a higher flow rate, and hence, the value of RF was lower. Comparing RF and μ_p for Barazan, RF was almost the same as the viscosity, and no additional effect was observed. By using the shear rate values in Table 4.9 together with Figures 4.2, 4.3 and 4.5, it was seen that the apparent viscosities (at 70 °C) were almost the same as the bulk viscosity (at 20 °C). Shear rates and apparent polymer viscosities were plotted with bulk viscosities, see Figure 4.26.

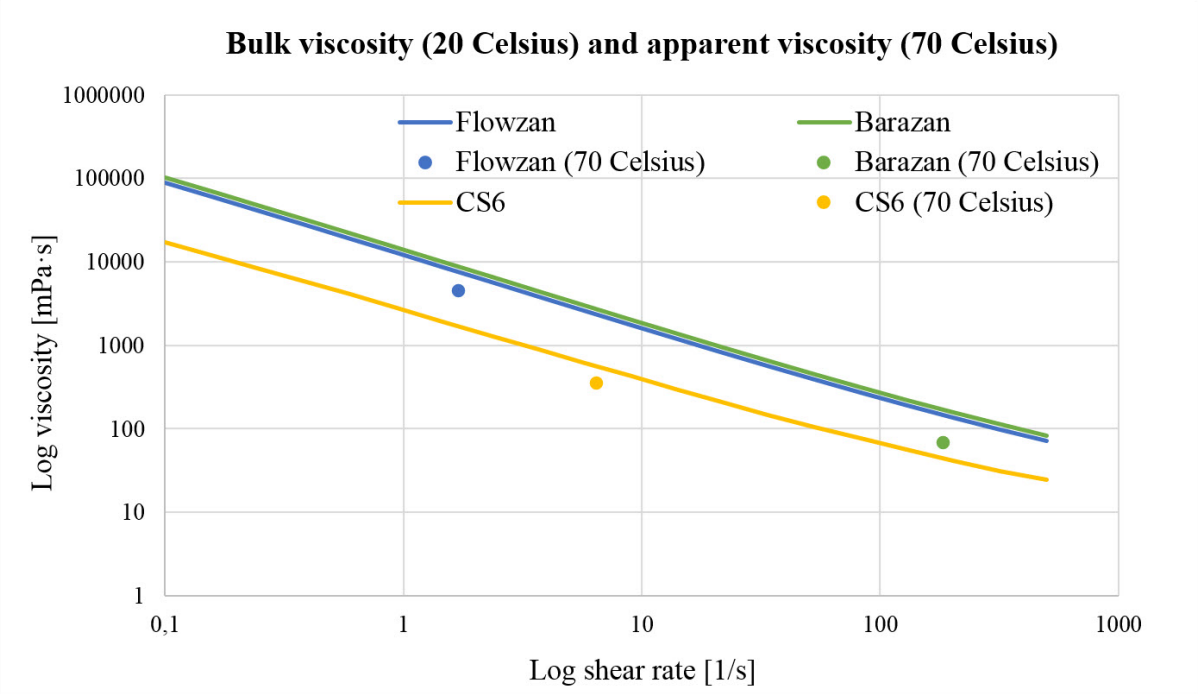

Figure 4.26: Bulk polymer viscosity at 20°C plotted together with apparent polymer viscosity at 70°C.

From filter tests and core flood experiment, it has been observed that Flowzan had poor filtration, at both 20 °C and 70 °C. When Flowzan was injected, it was seen that flow rate almost reached zero, and an effect of plugging was observed. Parameters from this core flood experiment, shows that criteria for disproportionate permeability reduction was fulfilled after the treatment, $RRF_o < RRF_w$.

For Scleroglucan, parameters in Table 4.9 indicated plugging in the core and a decreased flow rate was observed, see Figure 4.22. Filterability from filtration test at 20 °C was poor at all pressures and filter sizes. Filtration tests at 70 °C, on the other hand, showed excellent filterability. Because of excellent filtration at 70 °C with filter size 8 μm, it was a bit strange that poor filterability was shown in the core at the same temperature. Plugging in the core, may be explained by a smaller pore size distribution in the core (6 μm). Even though plugging may occurred, parameters from core flood experiments showed that $RRF_o > RRF_w$, which is a negative effect of disproportionate permeability reduction.

For Barazan, the core flood experiments showed a small reduction in flow rate. No additional effect of polymer plugging was observed in this core. DPR parameters analyzed from core flood experiments showed that $RRF_o > RRF_w$. The value of $\mathrm{RRF}_{w,1}$ for the core segment was also low compared to Flowzan.

Plugging could be caused by the molecular weight of polymers but from viscosity measurements it was found that all three Xanthan polymers had the same molecular weight. Hence, the good plugging of Flowzan compared to poor plugging of Barazan was caused by other reasons. Therefore, plugging may not be determined by the molecular weight of polymer but instead by impurities attached to the polymer. This is debris from the fermentation process and is expected to have similar thermal stability as the polymer (described in section 2.5). So, if these impurities were the reason for polymer plugging, it is very important to perform filtration tests before polymer type is chosen for DPR treatments. This because debris/impurities will vary from polymer to polymer and from vendors delivering the polymer. This was the case for Flowzan and Barazan where they are both biopolymer Xanthan but delivered from different vendors.

It was not straight forward to determine DPR effects from filtration tests and core flood experiments, but based on all these experiments, Flowzan was the polymer type with the best plugging properties and greatest DPR effects.

Filter cake

From core flood experiments it was observed that a reduction in relative permeability mainly occurred at the core inlet. For Flowzan injection, a thick filter cake was attached to the core inlet. From Table 4.4, RRF_w for inlet part was 90.3 with filter cake and a value of 34.1 without filter cake. Hence, the filter cake was responsible for a higher RRF_w value, and it is an important factor to achieve good DPR effects.

For Barazan core flood, the similar effect of filter cake was observed for RRF values, even though the filter cake was very small and Barazan showed very low (or zero) plugging.

4.4.1 Well productivity

Formation damage may occur as a result when fluids have invaded into a formation. This will affect the permeability and the situation will change from homogeneous to non-homogeneous. Damage from fluid invasion will not be evenly distributed in the invaded zone. In this case it was assumed that both the invaded zone (r_x) and the zone before treatment (r_e) were homogeneous. r_x defines the invaded radius. As mentioned earlier, the criteria for a DPR treatment is that oil and water flow are separated and producing from isolated layers. Therefore, isolated oil and water layers were solved separately by using their relative permeabilites before and after the treatment (k_w, k_o). Another known criteria for consideration of DPR treatment is that $PI_{rw} > PI_{ro}$ before treatment.

From the theoretical part, an expression for the radial productivity index was given. Since it is known that $\frac{k}{k_x} = RRF$, Equation (2.34) can be written:

$$PI_r = \frac{\ln(\frac{r_e}{r_w})}{(RRF - 1)\ln(\frac{r_x}{r_w}) + \ln(\frac{r_e}{r_w})} \tag{4.1}$$

Values from core flooding experiments shows that PI_r was decreased when RFF value was increased, and the same effect when invasion depth was increased.

RRF values from core flood experiments were used in Equation (4.1) and listed in Table 4.10. External radius, r_e, was set to 1000 m and well radius, r_w, was set to 0,1 m.

Results were plotted to illustrate the impact of invasion depth and RRF values.

Table 4.10: Productivity Index with different values of residual resistance factor and invasion depth.

$Core_{polymer}$	RRF	$PI_{rw}(r_x= 0.1)$	$PI_{rw}(r_x=1)$	$PI_{rw}(r_x=5)$	$PI_{rw}(r_x=10)$
Flowzan	$RRF_w = 12$	1	0.267	0.176	0.154
Flowzan (2)	$RRF_w = 23$	1	0.154	0.097	0.083
Barazan	$RRF_w = 7.5$	1	0.381	0.267	0.235
CS6	$RRF_w = 8$	1	0.364	0.252	0.222
$Core_{polymer}$	RRF	$PI_{ro}(r_x= 0.1)$	$PI_{ro}(r_x=1)$	$PI_{ro}(r_x=5)$	$PI_{ro}(r_x=10)$
Flowzan	$RRF_o = 8$	1	0.364	0.252	0.222
Barazan	$RRF_o = 24$	1	0.148	0.093	0.080
CS6	$RRF_o = 27$	1	0.133	0.083	0.071

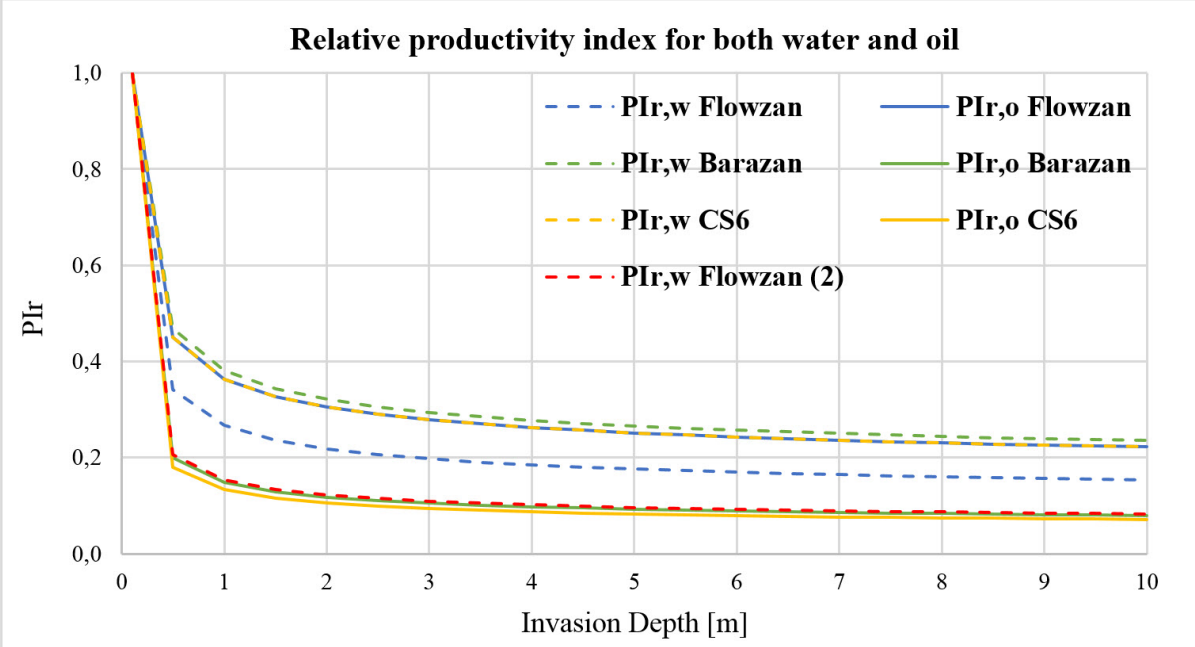

Figure 4.27: Relative productivity vs. invasion depth

Figure 4.27 clearly shows that PI_r decreased with an increasing invasion depth for constant RRF values. For r_x=r_w=0.1 the productivity index is equal to 1.

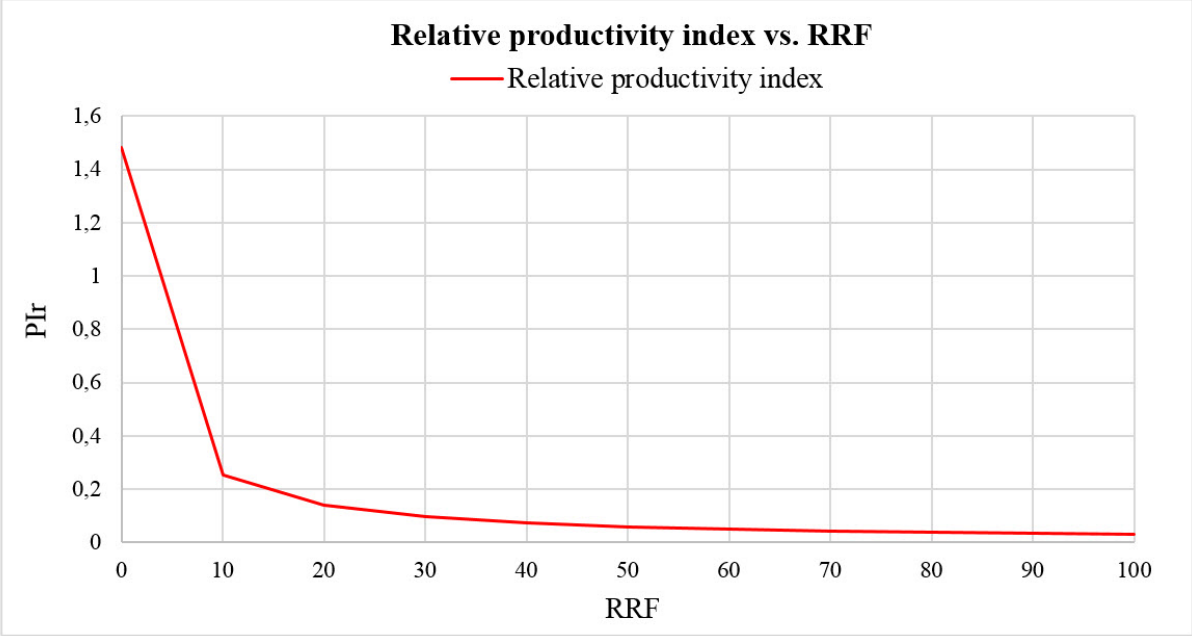

Figure 4.28: Relative productivity index vs. RRF

Figure 4.28 shows that the relative productivity index increased with increased RRF values. Invasion radius was set to r_x=2 m.

Criteria for successful DPR treatment ($PI_{ro} > PI_{rw}$) was achieved for injection with Flowzan, also notice that after the second time with Flowzan injection, RRF_w was higher and PI_{rw} was reduced even more.

Since PI_{ro} is depending on hydrostatic pressure and density difference between water and hydrocarbon phase, DPR treatments will be more efficient in deep wells with gas than shallow wells with oil. This is proved when PI_{ro} is solved from the following equation [Stavland, 2010]:

$$\Delta P_{hyd} = (\frac{gH(\rho_w - \rho_o)f_w(1-f_w)(PI_{ro} - PI_{rw})}{f_w PI_{rw} + (1-f_w)PI_{ro}}, \tag{4.2}$$

4.4.2 Alvheim Field parameters

Figure 4.29, represents the oil rate, liquid rate, bottom hole pressure (BHP) and an estimated productivity index before and after polymer injection in 2014 [Langaas and Stavland, 2019]. These Kneler data were used together with experimental data from the laboratory work to analyze field parameters.

Figure 4.29: Kneler well data from 2008-2019 [Langaas and Stavland, 2019].

Criteria for reduced water cut after a DPR treatment is that $\mathrm{PI}_{ro} > \mathrm{PI}_{rw}$ and $f_{w,1} < f_w$.

It is possible to look at an alternation of the fractional flow of water [Stavland, 2010]:

$$f_{w,1} = \frac{f_w PI_{rw}}{f_w PI_{rw} + (1 - f_w) PI_{ro}}, \tag{4.3}$$

where this equation gives an expression for a new water fraction, $f_{w,1}$, after treatment.

For simplicity, the friction part was omitted, and hence, drawdown pressure equals the hydrostatic pressure. Hydrostatic pressure, or lift pressure in the well, depends on fractional flow, f_w, and density of oil and water ρ_w, ρ_o. Two different lift pressures were given, before and after treatment:

$$P_{lift,0} = \Delta\rho g h(f_w), \tag{4.4}$$

and

$$P_{lift,1} = \Delta\rho g h(f_{w,1}). \tag{4.5}$$

$f_{w,1}$ is the new value of fractional flow after treatment, h, is the true vertical depth and, g, is the gravity. The lift pressure can be added to initial drawdown pressure, ΔP_0, and if it is assumed that BHP is the same, the pressure after treatment can be written:

$$\Delta P_1 = \Delta P_0 + \Delta\rho g h(f_w - f_{w,1}) + = \Delta P_0 + \Delta P_{lift}. \tag{4.6}$$

Then a criteria for increased oil production (using Equations (2.30) and (2.31)) is given by:

$$\frac{q_{o,0}}{q_{,1}o} = \frac{\Delta P_1}{\Delta P_0}\frac{\overline{k_o}}{k_o} = (1 + \frac{\Delta P_{lift}}{\Delta P_o})PI_{ro} > 1, \tag{4.7}$$

where $q_{o,0}$ and $q_{o,1}$ is the oil rate respectively before and after treatment and, $\dfrac{\overline{k_o}}{k_o} = PI_{r,o}$, shown in Equation (2.33).

Flowzan experimental results and Kneler data were used to calculate new water fraction and new oil production after the injection with Flowzan. From Figure 1.2, water fraction before polymer injection was given 0.68 (f_w=0.68). Before treatment, $\mathrm{PI}_o = 100\ \mathrm{Sm}^3/\mathrm{dbar}$ and liquid rate was q_o=2510 Sm^3/d (see Figure 4.29). In kneler well; h=2100 m (TVD) and the density difference was set to $\Delta\rho$=200 kg/m^3.

From Equation 4.3 - 4.7, water fraction and oil production rate were calculated, see Table 4.11. Invasion depth, r_x, was set to 1.5 m, r_e=1000 m and r_w=0.1 m.

From calculated parameters it clearly shows that water fraction was reduced ($f_{w,1} < f_w$) after injection of Flowzan. It also shows that the second injection of more Flowzan into the core gave even better results for DPR effects. Note that since a new value of RRF_o was

Table 4.11: Field parameters after Flowzan injection

Flowzan injection	$PI_{r,w}$	$PI_{r,o}$	$f_{w,1}$	ΔP_{lift} [bar]	ΔP_0 [bar]	$q_{o,1}/q_o$
First	0.24	0.33	0.60	3.30	25.10	0.37
Second	0.13	0.33	0.46	9.06	25.10	0.45

not measured after second time with Flowzan, the value from the first injection was used for RRF_o, and hence also for $PI_{r,o}$, after the second injection. Therefore, the second value of oil rate production is not 100 % correct but based on an assumption that RRF_o=8.

Table 4.11 above shows that the value of RRF_o (RRF_o=8), when 48 PV Isopar was backflooded (after first Flowzan injection), was to high to increase the oil production rate after the treatment. Since this value was still decreasing after 48 PV, an extrapolated line was used to illustrate a forecast of how much Isopar that was needed to be flooded back, to reach a value of RRF_o that would give increased oil production rate. Different values of RRF_o were tested to estimate when $q_{o,1}/q_o$>1, and following values were used:

- A value of RRF_o=1.3 was used in Equation (4.1).
- r_x=1.5 m, r_e=1000 m and r_w=0.1 m.
- PI_r(RRF_o=1.3) was then a value of 0.918.
- PI_r=0.918 used in Equation (4.7), with pressures listed in Table 4.11, resulted in increased oil production rate where:

$$\frac{q_{o,1}}{q_o} = (1 + \frac{3.3}{25.1})0.918 = 1.039 > 1. \tag{4.8}$$

Note that this was only calculated for the values representing the first injection of Flowzan.

The real values of RRF_o with Isopar backflooded were plotted, and by using the trendline it was calculated that when 204 PV (12275 ml) Isopar was flooded back, RRF_o=1.3, and the oil production rate would be increased (see Figure 4.30). Hence, the DPR treatment would be successful.

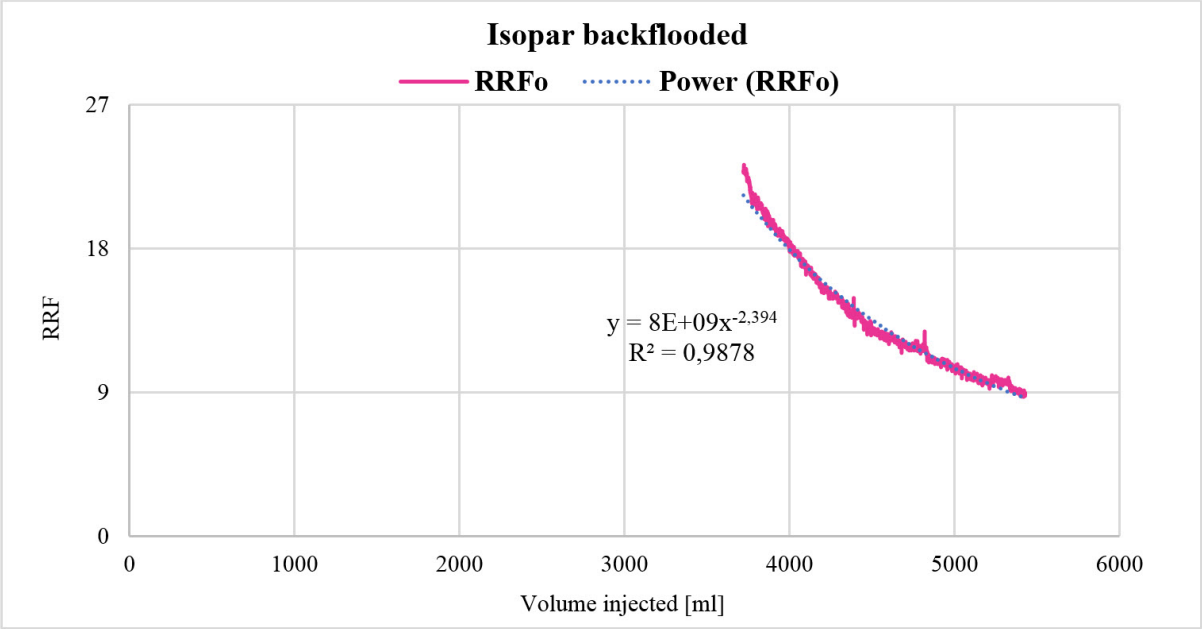

Figure 4.30: RRF vs. cumulative volume of Isopar, with Flowzan. Trendline used to estimate a forecasted volume of Isopar.

4.4.3 New residual oil saturation after polymer flooding

Polymer injection resulted in more oil produced, after the core was flooded to residual oil saturation (S_o=S_{or}). New values for residual oil saturation were calculated after all polymer floods, see Table 4.3 for exact values.

Relative permeability curves for a water-wet case is sketched in Figure 4.31. From this curve it is seen that a lower value of S_{or} will give a higher value of relative permeability for water, k_{rw}. A higher value of initial k_{rw} will increase the residual resistance factor for water, and improve DPR effects. A new value for initial water permeability was estimated from Corey-type permeabilities [Goda and Behrenbruch, 2004]:

$$k_{rw} = k_{rw,o}(\frac{S_w - S_{wi}}{1 - S_{wi} - S_{or}})^{n_w}, \tag{4.9}$$

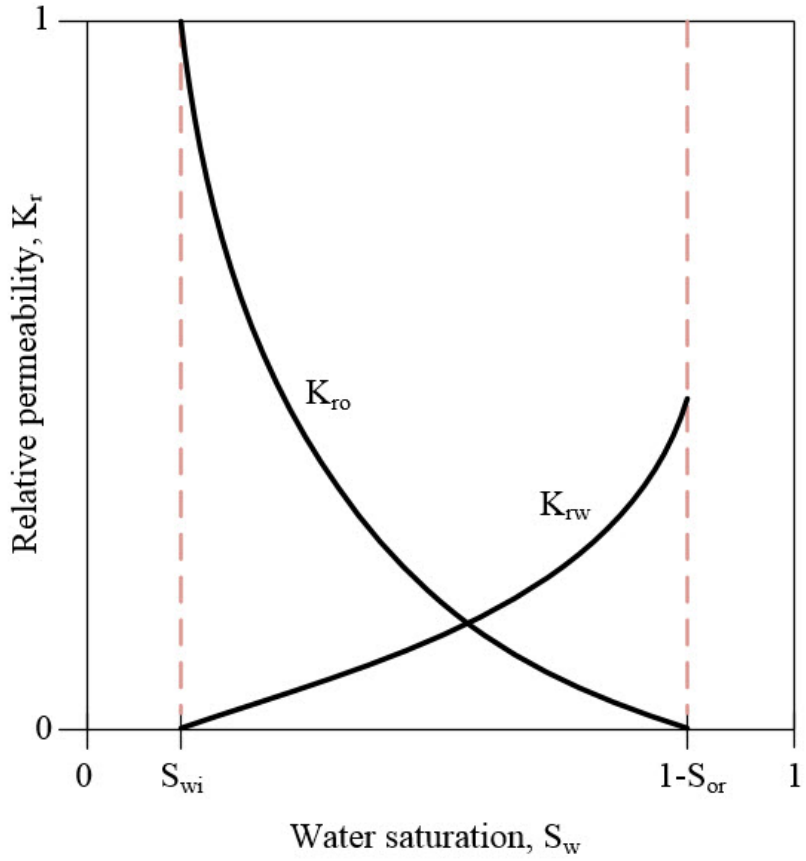

Figure 4.31: Relative permeability curves for a water-wet rock.

where:

- k_{rw} is the relative water permeability
- $k_{rw,o}$ is the end point relative water permeability
- S_w is water saturation
- S_{wi} is the irreducible water saturation
- S_{or} is the residual oil saturation
- n_w is the Corey exponent to water, here assumed to be n_w=2 for a water-wet rock.

For Flowzan where:

- k_{rw} = 0.14 D
- S_w = 1-S_{or} = 1-0.38 (water saturation before polymer injection)

- $S_{wi} = 0.12$
- $S_{or} = 0.35$ (new S_{or})
- $n_w = 2$

The new end point relative permeability was calculated to be $k_{rw,o} = 0.16$ D. Using the initial relative water permeability as 0.16, a new value of RRF_w for Flowzan after the first injection was RRF_w=13. This is not a very large difference from the earlier value (RRF_w=12), but it is important to know that a reduced value of S_{or} may impact DPR effects.

The reason that more oil was produced when polymer was injected can be explained by the capillary pressure. For a porous rock saturated with two phases, the pressure in the oil and water phase is related by the capillary pressure:

$$P_c(s_w) = P_o - P_w = \frac{2\sigma_{ow}cos(\theta)}{R}, \tag{4.10}$$

where, P_o and P_w, are the phase pressure for oil and water respectively. σ_{ow}, is the interfacial tension between oil and water, θ, is the wetting angle, and R, is the radius (see Figure 4.32). When polymer was injected, the entry capillary pressure for the small pore throat was exceeded and the trapped oil droplet was mobilized, and hence, more oil produced.

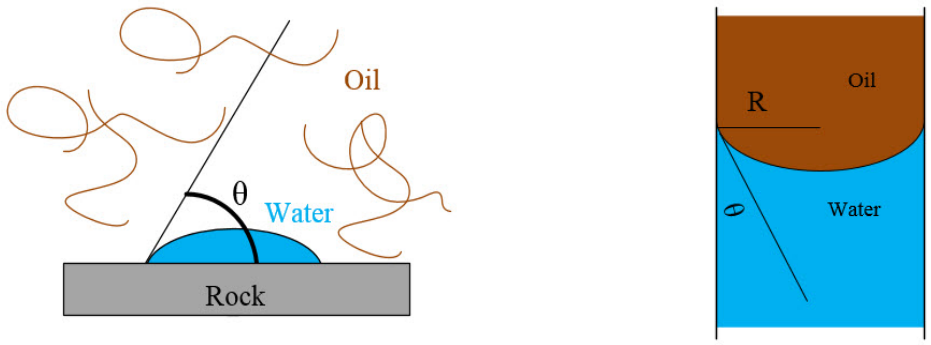

(a) Water-wet rock (b) Wetting angle and radius

Figure 4.32: Illustration of wetting angle and radius for a water-wet surface.

A ratio between the viscous and the capillary forces can be introduced as the capillary number (N_c):

$$N_c = \frac{u\mu_w}{\sigma_{ow}}, \tag{4.11}$$

where, u, is the flow velocity, μ_w, is the water viscosity and, σ_{ow}, is the interfacial tension between oil and water (or oil and polymer solution). In this case σ_{ow}=20 mN/m for all situations.

A capillary desaturation curve (CDC), is a curve describing the relationship between residual oil saturation and capillary number (N_c). This curve build its fundamental on flow conditions that are required for a good oil displacement in a porous medium related to oil recovery [Yeganeh et al., 2016].

The capillary number for Flowzan, Barazan and CS6 polymer flood were measured, see Table 4.12.

Table 4.12: Capillary number with polymer flooding

Polymer	N_c
Flowzan	5.5×10^{-4}
Barazan	4.9×10^{-4}
CS6	5.8×10^{-4}

Since more oil was produced after polymer flooding, it means that the capillary number (N_c) exceeded the critical capillary number that was given by:

$$N_c \geqslant \frac{\sqrt{\phi K}}{L\tau\sqrt{2}} = \frac{\sqrt{0.22 \times 100 \times 10^{-3}}}{1000 \times 3 \times \sqrt{2}} = 3.5 \times 10^{-5}, \tag{4.12}$$

where this critical capillary number was calculated for the porous cores used in this experiments. From the CDC below, see Figure 4.33, it shows that residual oil saturation becomes lower when the capillary number is larger than the value in Equation (4.12). Measured values of S_{or} (see Table 4.3) on y-axis are plotted against the calculated capillary numbers (see Table 4.12) on x-axis. This figure (Figure 4.33) also supports the observation from core flood experiments, where CS6 polymer flooding produced the highest amount of oil, and hence, resulted in a much lower value of S_{or}.

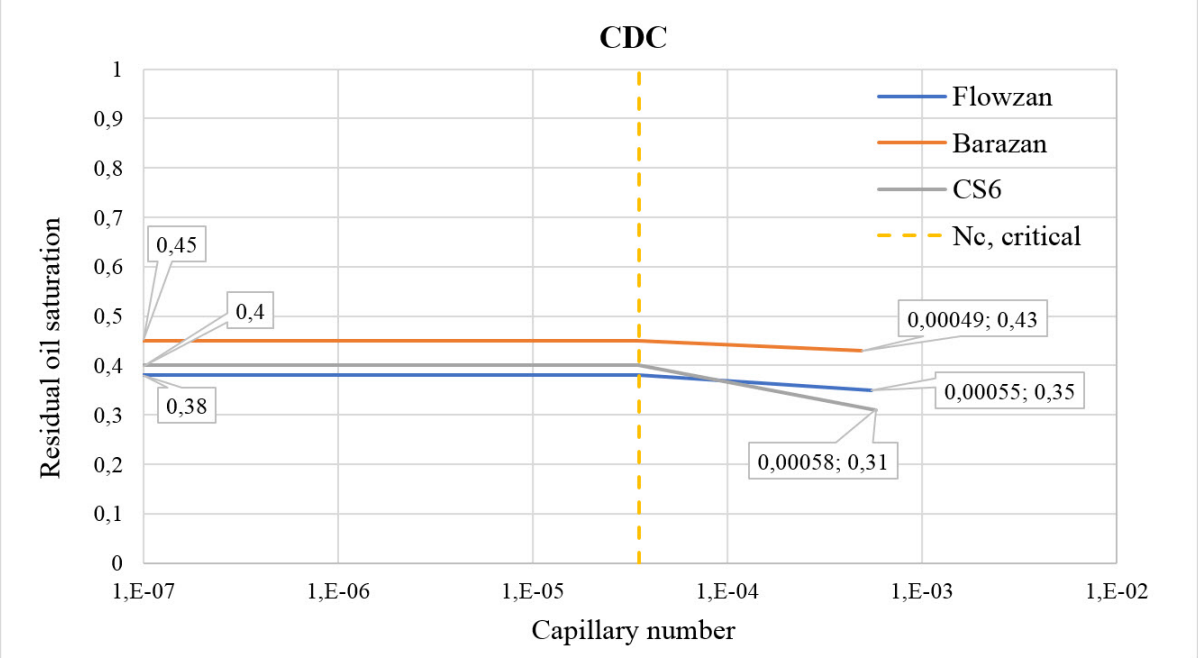

Figure 4.33: Capillary desaturation curve (CDC) showing S_{or} before and after polymer flooding with Flowzan, Barazan and CS6.

4.4.4 Comparing results with earlier work

Flowzan was tested in the earlier laboratory work initiated by Aker BP. From these experiments two parallel cores were used (one watered-out Bentheimer core and one oil-satureated Berea core). Flowzan was injected through both the parallel cores and after a shut-in period of 3 days, AFW brine was backflooded through the Bentheimer core and Isopar was backflooded through the Berea core. Results represented endpoint RRF_w=460 and endpoint RRF_o=10.2. DPR ratio was 45 and this value was still improving when the experiment was ended. The length of these cores were 7 cm while core length used in this experiment was 25 cm.

DPR results from experiments in this thesis, also shows that RRF_o <RRF_w for Flowzan, but RRF_w was a much lower value than seen before. As mentioned, Flowzan shows RRF_w values of 12 and 23. RRF_o value was 8, which is a smaller value than seen in the earlier experiment.

Flowzan injection shows DPR effects in both cases. The reason why the difference of RRF_w values were large may be explained by the difference in core length and the difference of polymer volume injected. In the earlier experiment more polymer was injected, and hence, more plugging may occurred into the core.

Since the values of RRF_o were almost the same, while RRF_w had a higher value where

a larger amount of polymer was injected, it seems like the polymer affects the water permeability in a greater extent than the oil permeability. Even though the value of RRF_o was large in the beginning, it seems to decrease as long as oil was produced. This was a positive effect for DPR evaluation.

4.4.5 Uncertainties

Uncertainties that occurred during the laboratory work needed to be taken into account when different parameters were calculated. In general, there are two type of uncertainties to distinguish between, systematic uncertainties and random uncertainties. Systematic uncertainties are describing errors in equipment and incorrect readings of measurements. Random uncertainties are uncertainties that will occur from error in one measurement to errors in the next measurements.

From this laboratory work, there were both uncertainties of the equipment that were used and from human readings of different measurements. The uncertainty in human errors from these experiments were assumed to be larger than uncertainties related to the equipment. Because of this, a list of human activities that could contribute to a certain uncertainty have been listed:

- Difference in amount of polymer solution on the rheometer during viscosity measurements. From plotted viscosity values, this measurements were very similar, and hence, this uncertainty was small.
- Temperature in the oven varied when doors were opened. This affected the flooding process.
- Readings of exact volume from separator; oil droplets in the water zone attached to the separator wall could give some error in volumes.
- Rounding of numbers in calculations of permeability and saturation.

To minimize errors and uncertainties in laboratory work, it is important that good procedures are written and that procedures are followed carefully.

Chapter 5

Conclusion

Properties for disproportionate permeability reduction and reduced water-cut with polymers have been tested. From these results it clearly shows that Flowzan is the best of the four candidates to use in DPR treatments at 70°C.

Filtration tests at room temperature showed that Flowzan and Barazan indicated some plugging, while CS6 showed total plugging. Filtration test (with 50 bar and filter size 8 μm) at 70 °C showed that Flowzan still indicated plugging of the filter while CS6 showed excellent filtration. Hence, Flowzan had poor filterability at both room temperature and at reservoir temperature.

From core flood experiments, Flowzan and CS6 showed plugging in the core but only Flowzan fulfilled the criteria: RRF_o <RRF_w. Barazan showed low (or approximately zero) plugging in the core and a negative DPR effect was seen; $RRF_o > RRF_w$.

Experimental Flowzan results were used together with Alvheim field data. Analysis of different parameters showed that the fraction of water in the field would have been reduced after the treatment. If approximately 204 PV Isopar was backflooded to a value of RRF_o=1.3 was reached, even the oil production rate would have been increased. This also supports the success criterion ($RRF_o < 2$) for a DPR fluid.

The filter-cake seen at the core inlet for cores flooded with Flowzan and Barazan contributed to a higher value of $\text{RRF}_{w,1}$. When the four core segments were backflooded with AFW it was observed that the permeability increased with the distance moving from the inlet, i.e. the permeability reduction depends on invasion depth.

Summarized disproportionate permeability reduction effects observed after the treatment with Flowzan were:

- $RRF_o < RRF_w$ (higher reduced water relative permeability than for oil relative permeability).
- $PIr, o > PI_{r,w}$ (higher relative productivity for oil).
- $f_w > f_{w,1}$ (reduced water fraction).
- $q_{o,1}/q_o$ >1 (increased oil production rate, if approximately 204 PV Isopar was backflooded).

From life-time estimation of Xanthan and Scleroglucan, an exponential decay has been used (section 2.5). Even though Scleroglucan had a higher thermal stability, the decay shows that Xanthan should last for several years (approximately 20 years) at a reservoir temperature of 70 °C.

Since all the Xanthan polymers had the same molecular weight, but different plugging properties, plugging can be explained by impurities/debris attached to the polymer. These impurities depends on the treatment processes of the polymer product and may vary from different vendors. Since poor filtration was caused by impurities, it is very important to perform filtration tests (and verify than FR>1) before a polymer product is selected for a DPR treatment.

Thus, based on this laboratory work, Flowzan should be recommended for a disproportionate permeability reduction treatment in the new pilot on the Alvheim field. This polymer showed poor filtration, and from core flood experiments the water phase permeability was reduced in a greater extent compared to the oil phase permeability. In the Alvheim reservoir, zones and baffles makes it possible to reduce the fraction of water and can contribute to an increased oil production from zones where remaining oil with low pressure support can be produced more efficient. The life-time of Xanthan (Flowzan) is expected to be of several years at a reservoir temperature of 70°C.

For further work, it can be recommended to perform a core flood experiment where oil is backflooded until a value of RRF_o has been stabilized, or until the value is low enough to increase the oil production. Backflooding of oil in each part of the divided core may also be of interest, to compare different values of $RRF_{o,i}$, where i is the core part (1, 2, 3 or 4).

Bibliography

[Abidin et al., 2012] Abidin, A., Puspasari, T., and Nugroho, W. (2012). Polymers for enhanced oil recovery technology. *Procedia Chemistry*, 4:11–16.

[Anton Paar Wiki, 2019] Anton Paar Wiki (2019). Basics of rheology. `https://wiki.anton-paar.com/en/basics-of-rheology/`. Accessed: 28.02.2019.

[Askarinezhad, 2018] Askarinezhad, R. (2018). *Produced Water Management*. University of Stavanger.

[Byron Bird et al., 2018] Byron Bird, R., Armstrong, R. C., and Hassager, O. (2018). *Dynamics Of Polymeric Liquids*. University of Stavanger.

[Goda and Behrenbruch, 2004] Goda, H. and Behrenbruch, P. (2004). Using a modified brooks-corey model to study oil-water relative permeability for diverse pore structures. paper spe 88538 presented at the spe asia pacific oil and gas conference and exhibition, perth, australia, 18-20 october.

[Kalpakci et al., 1990] Kalpakci, B., Jeans, Y., Magri, N., Padolewski, J., et al. (1990). Thermal stability of scleroglucan at realistic reservoir conditions. In *SPE/DOE Enhanced Oil Recovery Symposium*. Society of Petroleum Engineers.

[Kantzas, A and Bryan, J and Taheri, S,] Kantzas, A and Bryan, J and Taheri, S. Fundamentals of fluid flow in porous media. https://www.scribd.com/document/369641090/Fundamentals-of-Fluid-Flow-in-Porous-Media.

[Lake, 1989] Lake, L. W. (1989). *Enhanced oil recovery*. Old Tappan, NJ; Prentice Hall Inc.

[Langaas and Stavland, 2019] Langaas, K. and Stavland, A. (2019). Water shut-off with polymer in the alvheim field. Technical report, SPE-195485-MA.

[Littmann et al., 1992] Littmann, W., Kleinitz, W., Christensen, B., Stokke, B., Haugvallstad, T., et al. (1992). Late results of a polymer pilot test: performance, simulation

adsorption, and xanthan stability in the reservoir. In *SPE/DOE Enhanced Oil Recovery Symposium*. Society of Petroleum Engineers.

[Norsk Petroleum, 2019] Norsk Petroleum (2019). Norsk petroleum, alvheim. `https://www.norskpetroleum.no/fakta/felt/alvheim/`. Accessed: 21.03.2019.

[Oljedirektoratet, 2019] Oljedirektoratet (2019). Faktasider, alvheim. `http://factpages.npd.no/factpages/Default.aspx?culture=no`. Accessed: 27.03.2019.

[Seright et al., 2003] Seright, R., Lane, R., Sydansk, R., et al. (2003). A strategy for attacking excess water production. *SPE Production & Facilities*, 18(03):158–169.

[Simjoo et al., 2007] Simjoo, M., Vafaie Sefti, M., Dadvand Koohi, A., Hasheminasab, R., and Sajadian, V. (2007). Polyacrylamide gel polymer as water shut-off system: preparation and investigation of physical and chemical properties in one of the iranian oil reservoirs conditions. *Iranian Journal of Chemistry and Chemical Engineering (IJCCE)*, 26(4):99–108.

[Stavland, 2010] Stavland, A. (2010). How to apply the flow velocity as a design criterion in rpm treatments. *SPE Production & Operations*, 25(02):223–231.

[Sun et al., 2012] Sun, Y., Saleh, L., and Bai, B. (2012). Measurement and impact factors of polymer rheology in porous media. In *Rheology*. IntechOpen.

[Sydansk and Romero-Zerón, 2011] Sydansk, R. D. and Romero-Zerón, L. (2011). *Reservoir Conformance Improvement*. SPE.

[Sydansk et al., 2000] Sydansk, R. D., Southwell, G., et al. (2000). More than 12 years of experience with a successful conformance-control polymer gel technology. In *SPE/AAPG Western Regional Meeting*. Society of Petroleum Engineers.

[Thomas et al., 1998] Thomas, F. B., Bennion, D., Anderson, G., Meldrum, B., et al. (1998). Water shutoff treatments-reduce water and accelerate oil production. In *Annual Technical Meeting*. Petroleum Society of Canada.

[Yeganeh et al., 2016] Yeganeh, M., Hegner, J., Lewandowski, E., Mohan, A., Lake, L. W., Cherney, D., Jusufi, A., Jaishankar, A., et al. (2016). Capillary desaturation curve fundamentals. In *SPE Improved Oil Recovery Conference*. Society of Petroleum Engineers.

[Zolotukhin and Ursin, 2000] Zolotukhin, A. B. and Ursin, J.-R. (2000). *Introduction to Petroleum Reservoir Engineering*. Høyskoleforlaget AS.